

Research



Article submitted to journal

Subject Areas:

nuclear physics, neutrino physics

Keywords:Neutrinos, neutrino mass,
underground science, low radioactive
background experimental techniques,
neutrino mass ordering**Author for correspondence:**

A. W. P. Poon

e-mail: awpoon@lbl.govExperimental neutrino physics
in a nuclear landscapeD. S. Parno¹, A. W. P. Poon² and V. Singh³¹Department of Physics, Carnegie Mellon University,
Pittsburgh, Pennsylvania 15213, USA²Nuclear Science Division, Lawrence Berkeley
National Laboratory, Berkeley, California 94720, USA³Department of Physics, University of California,
Berkeley, California 94720, USA

There are profound connections between neutrino physics and nuclear experiments. Exceptionally precise measurements of single and double beta-decay spectra illuminate the scale and nature of neutrino mass and may finally answer the question of whether neutrinos are their own antimatter counterparts. Neutrino-nucleus scattering underpins oscillation experiments and probes nuclear structure, neutrinos offer a rare vantage point into collapsing stars and nuclear fission reactors, and techniques pioneered in neutrino nuclear-physics experiments are advancing quantum-sensing technologies. In this article, we review current and planned efforts at the intersection of neutrino and nuclear experiments.

1. Introduction

Nuclear physics is pivotal in the story of the neutrino, the lightest known matter particle in the universe. Wolfgang Pauli first proposed the neutrino's existence in 1930 to solve the longstanding mystery of the nuclear beta-decay spectrum [1], and Clyde Cowan and Frederick Reines discovered the particle experimentally at a nuclear reactor in 1956 [2]. At the same time, the neutrino is a tool for understanding nuclear physics, illuminating fusion reactions inside the Sun [3] and beta decays on Earth. Here, we consider nuclear physics to encompass phenomena dominated or driven by nuclear effects – nuclear decays, nuclear reactions and nuclear structure – especially at low energies.

In the past century of work, physicists have established [4] that the neutrino is a neutral, left-handed lepton; the anti-neutrino, conversely, is right-handed. The three neutrino flavour states (ν_e, ν_μ, ν_τ), associated with charged-lepton flavours, are linear superpositions of the three neutrino mass states (ν_1, ν_2, ν_3), with resultant flavour oscillation [5–7] dictated by the mixing angles of the Pontecorvo–Maki–Nakagawa–Sakata (PMNS) matrix U , by the splittings Δm_{ij}^2 between mass states, and by the ratio of the source-detector distance to the neutrino energy. Since the neutrino's only Standard Model interaction is via the weak force, its interaction cross sections are intimidatingly small, but are measurable. Despite this progress, however, many basic questions are unanswered. For example, what is the absolute scale and nature (Dirac or Majorana) of the neutrino mass? What is the ordering of the mass values, and is there CP violation in the neutrino sector? Do the three known neutrino flavours constitute the whole neutrino sector, or are there “sterile” neutrinos that do not feel the weak force?

This review is conceived as a snapshot of current experimental efforts that relate nuclear and neutrino physics. We begin with an examination of two nuclear laboratories for exploring neutrino physics: single- and double-beta decay. As explored in Sec. 2, nuclear beta decays (including electron-capture decays) permit a direct, kinematic probe of the absolute neutrino-mass scale. Recent work has significantly narrowed the laboratory limits on this quantity, a crucial input to both particle theory and cosmology. Meanwhile, in Sec. 3, we see that searches for neutrinoless double beta decay – a never-before-seen variant on the rare double beta-decay process, which is possible only if neutrinos are Majorana particles – are taking nuclear-physics experiments to new scales and levels of background control. In Sec. 4, we briefly survey additional intersections of neutrino and nuclear physics, including the nuclear physics of high-energy neutrino interactions, essential for interpreting long-baseline neutrino-oscillation experiments (Sec. 4(a)); the use of low-energy neutrino scattering to illuminate nuclear properties and supernova nucleosynthesis (Sec. 4(b)); neutrino probes of fission reactors (Sec. 4(c)); searches for sterile neutrinos (Sec. 4(d)); and applications in quantum sensing (Sec. 4(e)).

2. Absolute neutrino-mass measurement

Neutrino-oscillation experiments have established that neutrinos cannot all be massless, but are insensitive to the individual mass eigenvalues m_i . To date, oscillation data are consistent with two options for neutrino-mass ordering: $m_3 > m_2 > m_1$ (normal ordering) and $m_2 > m_1 > m_3$ (inverted ordering). In either ordering, the mass of the lightest neutrino sets a scale for the others, which can be probed via studies of β and $\beta\beta$ decays (Sec. 3), and via cosmological observations. Some of these measurements are model-dependent. For example, the measured sum of the neutrino masses from cosmological studies — $\sum_i m_i$ — varies conspicuously under different model assumptions and data inputs, albeit achieving remarkable constraints [4]. The measurements described in this section are essentially model-independent.

Since Fermi established the kinematic relationship between the electron energy spectrum of the neutrino mass and β decay [8], many experiments have tried to determine the neutrino mass via β and electron-capture decays in different nuclei. Here, we focus on recent efforts and refer the reader to Ref. [9] for complete historical context.

Such probes of the neutrino-mass scale derive their sensitivity from precise spectral-shape measurements near the kinematic endpoint of the decay spectrum, where the presence of a non-zero neutrino mass appreciably changes the energy available to other particles in the final state. In the quasi-degenerate regime, where the mass scale is large compared to the mass splittings, kinematic experiments measure an effective neutrino mass m_β :

$$m_\beta^2 = \sum_i |U_{ei}|^2 m_i^2. \quad (2.1)$$

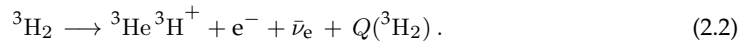
Since the fraction of β -decays in the small, sensitive energy interval δE below the endpoint energy $E_0 \approx Q$ (the Q -value of the decay), is proportional to $\left(\frac{\delta E}{Q}\right)^3$, an ideal nucleus for this type of measurement has a small Q -value, a relatively short half-life for the enhancement of source intensity, and a well-understood decay structure.

The isotopes used in current neutrino-mass measurement efforts are ^3H (Sec. (a)) and ^{163}Ho (Sec. (b)). Each has some complexity in the measured spectrum. In β -decay experiments with molecular ^3H , the final-state electronic, vibrational, and rotational excitations modify the beta spectrum significantly and are obtained from theory. In ^{163}Ho electron-capture experiments, similarly intricate theoretical calculations are needed to account for X-ray, Auger-Meitner, and Coster-Kronig transitions, as well as nuclear recoil.

Recent efforts have identified other possible isotopes with ultralow Q -values (< 1 keV), and thus enhanced statistical sensitivity; see Ref. [10] for a review. These isotopes, however, typically have extremely long lifetimes, complex nuclear structures, and very small branching ratios for the specific decay modes with ultralow Q , rendering them impractical targets for future precise experiments.

(a) ^3H

The best current kinematic limit on the neutrino-mass scale arises from the decay of molecular tritium, $^3\text{H}_2$:



The differential decay rate, summed over all final molecular states f in the daughter molecule, each with energy V_f and weighted by the transitional probability P_f to that state, is [11]:

$$\begin{aligned} \frac{d\Gamma}{dE} = & \frac{G_F^2 |V_{ud}|^2}{2\pi^3} |M_{\text{nuc}}|^2 F(Z, E) \cdot p(E + m_e) \\ & \cdot \sum_f P_f \epsilon_f \sqrt{\epsilon_f^2 - m_\beta^2} \Theta(\epsilon_f - m_\beta), \end{aligned} \quad (2.3)$$

where G_F is the Fermi coupling constant, and $|V_{ud}| = 0.97373 \pm 0.00031$ is the CKM matrix element [4]. M_{nuc} is the nuclear transition matrix element. $F(Z, E)$ is the Fermi function that accounts for the Coulomb interaction between the outgoing electron with kinetic energy E and momentum p , and the daughter nucleus with atomic charge Z ; ϵ_f is the neutrino energy ($= E_0 - V_f - E$); E_0 is the maximum β energy if the neutrino mass is zero, and the Heaviside step function $\Theta(\epsilon_f - m_\beta)$ ensures energy conservation.

The KARlsruhe TRItium Neutrino (KATRIN) experiment [12] is the most sensitive operating direct neutrino-mass experiment, and the current best limit of $m_\beta < 0.8$ eV/ c^2 (90% C.L.) is based on its first two measurement campaigns [13]. In the KATRIN apparatus, cold $^3\text{H}_2$ gas is injected into the windowless source section. The decay electrons are guided by magnetic fields to the main spectrometer for energy analysis. Differential and cryogenic pumping stages along the beamline reduce the tritium flow by 14 orders of magnitude. The electrons' transverse momentum is adiabatically transformed into longitudinal momentum in a slowly varying magnetic field, which reaches a minimum in the "analysing" plane of the main spectrometer. Only electrons with enough kinetic energy to pass the potential barrier of ~ -18.6 kV are transmitted to the detector. Essentially, the main spectrometer acts as a high-pass filter so that the detector records

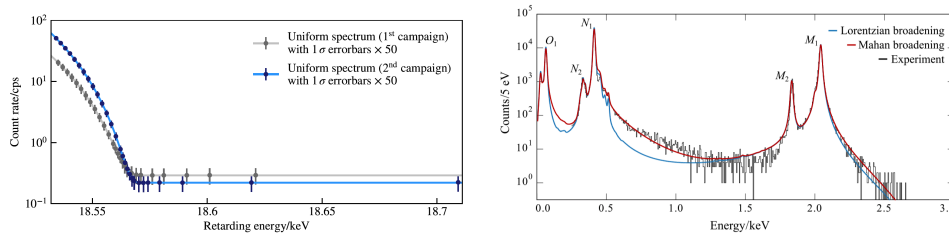


Figure 1. Measured integral ${}^3\text{H}$ β spectrum near the endpoint from the KATRIN experiment [13] (left) and the differential electron-capture calorimetric spectrum of ${}^{163}\text{Ho}$ from the ECHO experiment [16] (right).

an integral spectrum (Fig. 1, left). KATRIN continues to take data toward a design sensitivity goal of $m_\beta < 300$ meV.

The statistical sensitivity of a KATRIN-type experiment follows [14]:

$$\delta m_\beta^2 \propto \frac{b^{\frac{1}{6}}}{r^{\frac{2}{3}} t^{\frac{1}{2}}} \quad (2.4)$$

where b is the background rate, r is the radius of the spectrometer, and t is the measurement time. KATRIN observes higher-than-expected backgrounds arising from low-energy electrons generated in the large volume of the main spectrometer; even without this issue, the diameter of a spectrometer to improve on KATRIN's sensitivity by an order of magnitude would be unrealistically large. Instead of enlarging the spectrometer, improvements to a KATRIN-like experiment would thus require reducing the background or changing the role of the main spectrometer in the measurement, e.g. by operating in a time-of-flight mode [15].

It is clear from Eq. 2.3 that the molecular final-state distribution (FSD) populated by ${}^3\text{H}_2$ decay affects the measured β spectrum, and hence m_β^2 . Near the spectral endpoint, any unaccounted-for Gaussian broadening $\Delta\sigma$, including that of the FSD, changes the extracted m_β^2 by [17]:

$$\Delta m_\beta^2 \approx -2\Delta\sigma^2. \quad (2.5)$$

In fact, it has been demonstrated using Eq. 2.5 that the use of a more sophisticated, modern FSD [18] is enough to render negative m_β^2 results from the 1980s consistent with zero [19]. Significant theoretical effort has been invested in improved FSD calculations, consistent with the limited available experimental tests [19,20], and the resulting uncertainty is now negligible for KATRIN. However, the spectral broadening induced by the FSD would become a significant limiting factor for experiments with sufficiently sharp energy resolution.

Cyclotron Radiation Emission Spectroscopy (CRES), an alternative to the KATRIN strategy, is a frequency technique for determining m_β by precisely measuring the cyclotron radiation from the relativistic electron in atomic ${}^3\text{H}$ β decay [21]. The power radiated by an 18-keV electron in a 1 T field is approximately 1 fW. The Project 8 experiment aims to realise this concept by measuring the differential energy spectrum of atomic ${}^3\text{H}$, thereby eliminating the FSD broadening of molecular ${}^3\text{H}_2$ and the need for a mammoth spectrometer.

In its first milestone, the Project 8 experiment observed single electrons from ${}^{83\text{m}}\text{Kr}$ decay [22]. Recently, the experiment has demonstrated CRES as a viable technique for a low-background neutrino-mass measurement with ${}^3\text{H}_2$ in a small trap, setting a Bayesian upper limit of $m_\beta < 155$ eV/ c^2 (90% C.L.). No background was observed after 82 days of running, and an adequate resolution was demonstrated using ${}^{83\text{m}}\text{Kr}$ 17.8-keV internal-conversion electrons [23, 24]. The collaboration is now following two parallel research-and-development (R&D) tracks: scaling up the CRES technique to larger volumes with resonant cavities, and developing an atomic tritium source in which magnetic trapping of ${}^3\text{H}$ atoms prevents recombination. The ultimate

goal of the Project 8 experimental programme is a sensitivity of $m_\beta < 40 \text{ meV}/c^2$ (90% C.L.) with atomic ^3H .

(b) ^{163}Ho

Serious non-tritium-based efforts to the neutrino mass currently centre on the internal-bremsstrahlung electron-capture (IBEC) decay spectrum of ^{163}Ho to ^{163}Dy , as first proposed in Ref. [25]. Earlier calorimetric measurements of the ^{187}Re beta-decay spectrum have been abandoned due to difficulties in designing a suitable, scalable detector [26]. Despite its relatively low Q -value, ^{187}Re has an exceptionally long half-life ($4.3 \times 10^{10} \text{ y}$) due to its first-order forbidden transition. But the ^{187}Re programme had significantly advanced the development of the ^{163}Ho experiments; in particular, in microcalorimetry.

In ^{163}Ho measurements, microcalorimeters capture the de-excitation electrons and photons of the daughter $^{163}\text{Dy}^*$ entirely and convert them to heat. The neutrino mass is manifested in the upper end of the $^{163}\text{Dy}^*$ deexcitation spectrum, similar to the modification in β -decay spectra near the endpoint. The synthetic isotope ^{163}Ho has a low $Q = 2.833 \text{ keV}$ [27] and a half-life of 4570 years. Since neutrinos are emitted in electron-capture decays instead of antineutrino emission in ^3H decay, the two types of measurement are complementary. The ^{163}Ho spectrum has a complex shape (Fig. 1) requiring a careful treatment of resonance features, shake-off electrons, and solid-state effects from the absorber [28]. The pile-up rate in the microcalorimeters can be very high as they measure the full differential spectrum. Different ^{163}Ho experiments deploy different SQUID-based detector technologies to read out minute temperature changes. HOLMES [29] uses Transition Edge Sensor (TES) arrays, while ECHo uses arrays of magnetic metallic calorimeters (MMCs) and has set a limit of $m_\beta < 150 \text{ eV}/c^2$ (95% C.L.) [16]. HOLMES has recently measured its first ^{163}Ho decay spectrum. The ECHo-1k phase of the programme will reach a neutrino-mass sensitivity below $20 \text{ eV}/c^2$; its next phase, ECHo-100k, is projected to reach a sensitivity below $2 \text{ eV}/c^2$ [30]. An international consortium has recently called for an effort of neutrino-mass measurement in ^{163}Ho with sub-eV sensitivity [31].

3. Neutrinoless double-beta decay

It is not currently understood how the existence of neutrino mass should be incorporated into the Standard Model. Since the neutrino has no electric charge, both Dirac and Majorana mass terms are possible. The search for neutrinoless double-beta decay ($0\nu\beta\beta$) is the only practical means to establish which best describes the neutrino nature.

In the Standard Model, double-beta decay ($2\nu\beta\beta$) is an allowed second-order decay process in which two uncorrelated nucleons decay simultaneously and emit two electrons and two anti-neutrinos: $(Z, A) \rightarrow (Z + 2, A) + 2e^- + 2\bar{\nu}$. However, if neutrinos are their own antiparticles (Majorana particles [32]), the emitted anti-neutrino from one of the nucleons can be absorbed in the second interaction so that there are no neutrinos in the final state:

$$(Z, A) \rightarrow (Z + 2, A) + 2e^-. \quad (3.1)$$

This is the much sought-after $0\nu\beta\beta$ decay mode, which violates lepton-number conservation – an accidental symmetry of the Standard Model – and could help explain the matter-antimatter asymmetry in our Universe [33]. The $0\nu\beta\beta$ decay rate can be expressed as

$$[T_{\frac{1}{2}}^{0\nu}]^{-1} = \sum_i G_i^{0\nu}(Z, Q) \cdot |M_i^{0\nu}|^2 \cdot \zeta_i^2 \quad (3.2)$$

where $G^{0\nu}(Z, Q)$ is the phase-space factor that depends on the proton number (Z) of the decaying nucleus and the Q -value of the decay, $M_i^{0\nu}$ is the nuclear matrix element (NME), and ζ_i depends on the mechanism and mode of the lepton-number-violating process. The phase-space factors have been calculated [34,35] and the Q -values have been measured precisely for several isotopes actively pursued by experiments [36–39]. If we assume that the decay is mediated by the exchange

of light Majorana neutrinos, ζ reduces to an effective Majorana neutrino mass $m_{\beta\beta}$, which is a coherent sum of neutrino mass eigenvalues defined as

$$|m_{\beta\beta}| = \left| \sum_{i=1}^3 U_{ei}^2 m_i \right| \quad (3.3)$$

Fig. 2 shows the relationship between $m_{\beta\beta}$ and m_β (Sec. 2).

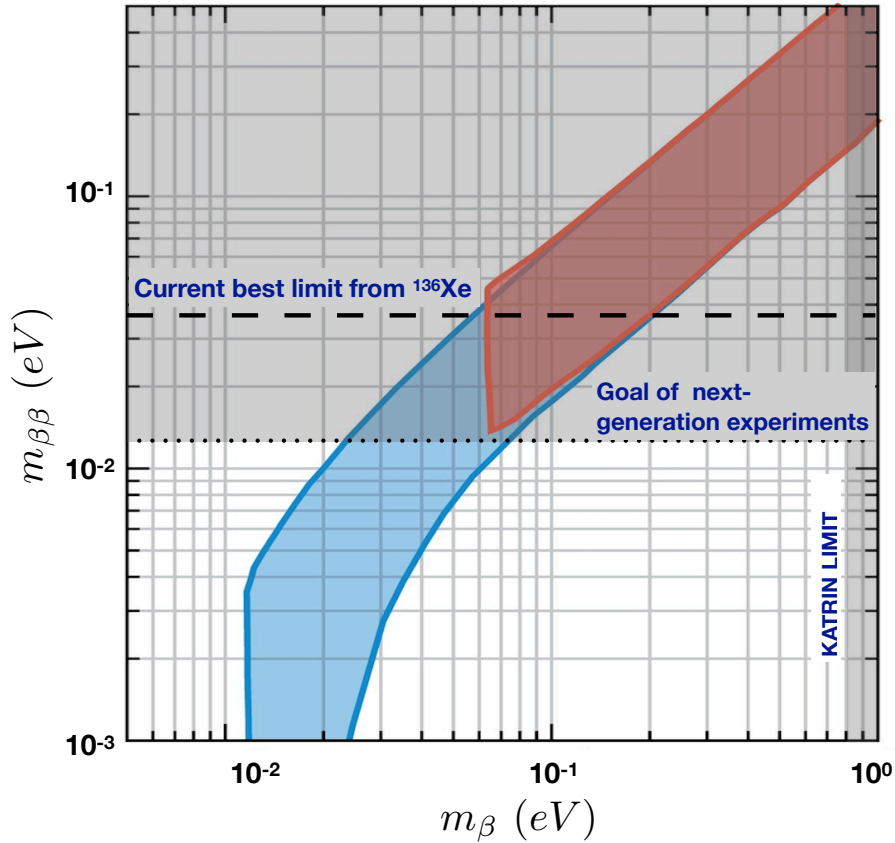


Figure 2. The effective Majorana-mass observable $m_{\beta\beta}$ in neutrinoless double-beta decay searches vs. the direct kinematic observable m_β . The neutrino mixing parameters $U_{\alpha i}$ are varied within their ranges from oscillation experiments. The blue area is for the normal mass ordering, while the red area is for the inverted mass ordering. The next generation of $0\nu\beta\beta$ experiments aims to probe the entire inverted mass ordering through $m_{\beta\beta}$. Adapted from [40].

In the scenario of light-neutrino exchange, the decay rate is written as [41,42]:

$$[T_{\frac{1}{2}}^{0\nu}]^{-1} = G^{0\nu}(Z, Q) \cdot (g_A)^4 \cdot |M^{0\nu}|^2 \cdot \frac{m_{\beta\beta}^2}{m_e^2} \quad (3.4)$$

where g_A is the axial-vector coupling constant factored out of the nuclear matrix element $|M^{0\nu}|^2$, and m_e is the mass of the electron. The corresponding NMEs are calculated using various macroscopic and microscopic nuclear models dealing with complex nuclear structures (Sec. (e)). However, the predictions from these nuclear models disagree by more than a factor of two [41], which results in a significant uncertainty on the predicted value of $m_{\beta\beta}$. While the constraint on neutrino mass through $0\nu\beta\beta$ is model-dependent, establishing the Majorana character is not; the

Black-Box Theorem [43–45] states that the observation of neutrinoless double-beta decay would directly imply lepton-number violation.

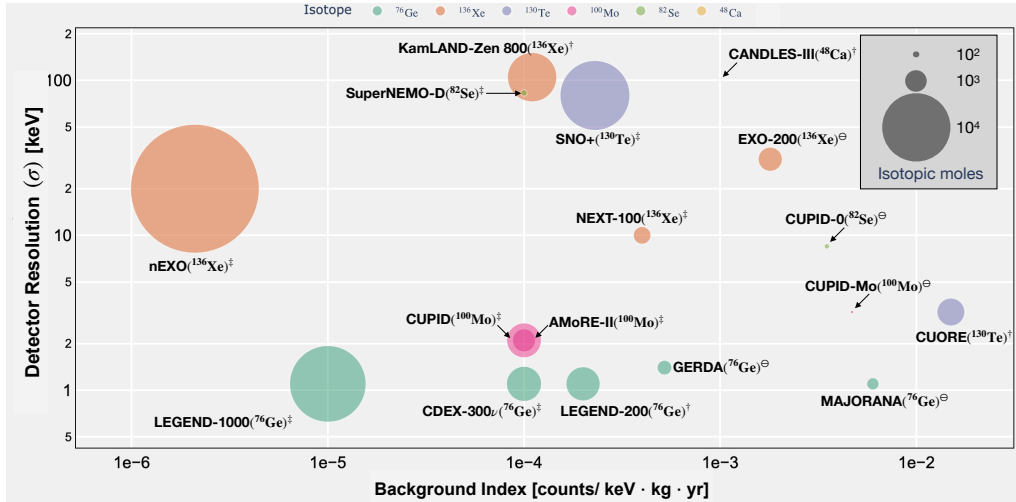


Figure 3. Relevant experimental parameters – background index, detector resolution (σ), and isotopic moles – for recently completed (\ominus), currently running (\dagger), and proposed (\ddagger) $0\nu\beta\beta$ -decay search experiments. Furthermore, isotopes with high $Q_{\beta\beta}$ value offer an additional advantage since the phase space factor $G^{0\nu}(Z, Q)$ is proportional to $Q_{\beta\beta}^5$ and radioactive backgrounds tend to be smaller at higher energy.

The fundamental concept behind a $0\nu\beta\beta$ search involves detecting two emitted electrons and identifying their summed energy peak at the Q -value ($Q_{\beta\beta}$) of the energy spectrum. Typically, the Q -values of relevant isotopes are precisely known and the search for a $0\nu\beta\beta$ peak is limited to a narrow energy range determined by the detector's energy resolution (ΔE) at $Q_{\beta\beta}$. The search sensitivity is also limited by background events that mimic the signal signature in the region of interest (ROI). The half-life sensitivity of an experiment can be expressed as [46]:

$$\begin{aligned}
 T_{1/2}^{0\nu} &\propto \epsilon \cdot \sqrt{\frac{M \cdot t}{B \cdot \Delta E}} && \text{background-limited} \\
 T_{1/2}^{0\nu} &\propto \epsilon \cdot M \cdot t && \text{background-free}
 \end{aligned} \tag{3.5}$$

where ϵ is the detector's efficiency, M is the mass of the isotope deployed, and B is the background index, typically expressed as the number of background events expected in a certain energy range within the live-time of the experiment (t) for a given detector mass. It is often reported in units of counts per detector mass, energy, and time, *e.g.* counts/(keV·kg·year).

Given the extreme rarity of this decay, the experimental challenge lies in detecting this process amidst a background of other radioactive decays and cosmic rays [47]. Experiments are carried out in deep underground facilities [48] that provide a natural barrier against cosmic-ray interference. The dominant sources of radioactive background typically include α , β , and γ radiation from primordial decay chains, together with neutron-induced reaction products in underground labs. Experiments using isotopes with $Q_{\beta\beta} > 2615$ keV benefit from a lower background by avoiding the ^{208}Tl line. However, it is not always possible to deploy these isotopes on a large scale due to their low isotopic abundance or a lack of suitable detector technology with low enough background levels.

Some of the world's leading limits on $0\nu\beta\beta$ decay were obtained with experiments using ^{76}Ge , ^{136}Xe , and ^{130}Te – all with $Q_{\beta\beta} < 2615$ keV – using very powerful detection and background-rejection techniques. These experiments use materials with low radioactive content

in detector construction, minimising internal background sources while employing layers of passive shielding to reduce external backgrounds. Experiments employing water or liquid cryogens for passive shielding can use the same medium as an active veto for cosmic rays. Active background rejection, using such techniques as timing, event topology, fiducialisation of the active detector volume, and particle identification, complements passive methods.

Table 1. Comparison of lower half-life limits $T_{1/2}^{0\nu}$ (90% CL) and corresponding $m_{\beta\beta}$ limits for the recently completed, currently running, and next-generation proposed experiments. Each range of $m_{\beta\beta}$ upper limits is as reported by that experiment and depends on their choice of multiple matrix elements. The measured sensitivities are reported in bold for contrast with projected sensitivities.

Experiment	Status	Isotope	$T_{1/2}^{0\nu}$ [yr]	$m_{\beta\beta}$ [meV]
GERDA [49]	Completed	^{76}Ge	1.8×10^{26}	79—180
MAJORANA [50]	Completed	^{76}Ge	8.5×10^{25}	113—269
LEGEND-200 [51]	Taking Data	^{76}Ge	1.5×10^{27}	34—78
LEGEND-1000 [51]	Proposed	^{76}Ge	8.5×10^{28}	9—21
CDEX-300 ν [52]	Proposed	^{76}Ge	3.3×10^{27}	18—43
KamLAND-Zen [53]	Taking Data	^{136}Xe	2.3×10^{26}	36—156
EXO-200 [54]	Completed	^{136}Xe	3.5×10^{25}	93—286
nEXO [55]	Proposed	^{136}Xe	1.3×10^{28}	6.1—27
NEXT-100	Construction	^{136}Xe	7.0×10^{25}	66—281
CUORE [56]	Taking Data	^{130}Te	2.2×10^{25}	90—305
SNO+ [57]	Construction	^{130}Te	2.1×10^{26}	37—89
AMoRE-II [58]	Proposed	^{100}Mo	5.0×10^{26}	17—29
CUPID-Mo [59]	Completed	^{100}Mo	1.8×10^{24}	280—490
CUPID [60]	Proposed	^{100}Mo	1.5×10^{27}	10—17
CUPID-0 [61]	Completed	^{82}Se	4.6×10^{24}	263—545
SuperNEMO-D [62]	Construction	^{82}Se	4.0×10^{24}	260—500
CANDLES-III [63]	Taking data	^{48}Ca	5.6×10^{22}	2900—1600

Figure 3 shows the recently completed, running, and proposed experiments in terms of achieved or projected background indices, detector resolution, and the amount of target isotope used. A comparison of the lower half-life limits and corresponding $m_{\beta\beta}$ values is given in Table 1. Although $0\nu\beta\beta$ decay has not been observed, the current generation of experiments has successfully deployed several hundreds of kilogrammes of isotopes to push the $T_{1/2}^{0\nu}$ lower limit in the order of 10^{25} — 10^{26} years despite being background-limited. The next generation of experiments seeks to increase the isotope mass significantly (\approx tonne-scale). Since the sensitivity in a background-free experiment scales linearly with measurement time t instead of \sqrt{t} , these experiments aim to reduce background levels by several orders of magnitude. Deploying a “ton-scale” detector and considerably decreasing the background will allow next-generation experiments to probe half-lives in the range of 10^{26} — 10^{28} years with typically ten years of data taking, setting a limit of $m_{\beta\beta} < (18.4 \pm 1.3)$ meV [64] and ruling out the inverted hierarchy of neutrino mass spectra. We reiterate that this interpretation of half-life limits in terms of $m_{\beta\beta}$ is only valid under the standard assumption that the decay is mediated by light Majorana neutrino exchange, and all other mechanisms that could result in $0\nu\beta\beta$ decay are considered negligible or nonexistent.

It is essential to search for $0\nu\beta\beta$ in multiple isotopes not only for confirmation of discovery but also to identify the underlying mechanism of decay [65–68]. Experiments using different isotopes provide varying search sensitivity and background discrimination capabilities and are subject to independent systematic uncertainties. Measurements of multiple isotopes, therefore, not only allow cross-validation of theoretical models across different nuclear environments but also help

identify and control experimental systematic uncertainties. In addition, precise measurements of diverse two-neutrino processes are needed to refine NME calculations and provide a comprehensive grasp of the Standard Model background in $0\nu\beta\beta$ searches. Consequently, technologies that can reconstruct individual energies and topologies (e.g., SuperNEMO [62]) will have a crucial role even if they may not allow significant scaling up of isotopic mass. Analogously, the light $\beta\beta$ emitter ^{48}Ca , which has extremely low isotopic abundance (0.2%) and will be extremely cost-intensive to scale up, is an interesting nucleus to probe since it is an ideal target for benchmarking various NME calculations (Sec. (e)).

Numerous review articles summarise the massive experimental and theoretical efforts over the last couple of decades [40,69–73]. Here, we take a bird’s-eye view of the experimental landscape for $0\nu\beta\beta$ -decay searches, focusing on efforts toward future ton-scale experiments. We refer the reader to Fig. 3 and Table 1 for the relevant experimental parameters. Different isotopes offer distinct advantages and challenges regarding experimental criteria of scalable detector technology that can provide comprehensive sensitivity and background discrimination.

(a) ^{76}Ge ($Q_{\beta\beta} = 2039.0$ keV)

The GERmanium Detector Array (GERDA) experiment [49] was located at the Laboratori Nazionali del Gran Sasso (LNGS), Italy. Its high-purity germanium detectors (HPGe) were enriched to 87% of the isotope ^{76}Ge and immersed and cooled directly in ultra-pure liquid argon (LAr), whose scintillation also actively vetoed radioactive backgrounds. GERDA achieved the lowest background sensitivity ($\text{BI} \times \sigma$) obtained by any $0\nu\beta\beta$ -decay search. The MAJORANA DEMONSTRATOR (MJD) [50] at the Sanford Underground Research Facility (SURF), USA, took a more conventional approach with layered ultralow-background electroformed copper (EFCu) and lead shielding for HPGe detectors housed in EFCu vacuum cryostats. MJD reported the best detector resolution among all $0\nu\beta\beta$ -decay searches with ~ 1.1 keV (σ) at $Q_{\beta\beta}$.

The next-generation Large Enriched Germanium Experiment for Neutrinoless $\beta\beta$ Decay (LEGEND) [51] aims to achieve a sensitivity of $T_{\frac{1}{2}}^{0\nu} > 10^{28}$ yr by combining the best of GERDA and MJD technologies. The goal is to operate 1 ton of enriched germanium detectors for 10 years at a background index of $\sim 1 \times 10^{-5}$ counts/kg-keV-yr. The programme is being pursued in phases, with LEGEND-200 currently deployed and taking data in an upgraded GERDA infrastructure. LEGEND-200’s projected background index is about three times lower than GERDA, mainly due to fewer cables and electronic components per unit mass of HPGe detectors, an improved light readout for the liquid-argon veto, and improvements in the radiopurity of construction materials. LEGEND-1000 envisages reducing the background index by another factor of 20 by using underground argon (with a reduced level of radioactive ^{42}Ar) for shielding, and further reducing the radioactivity levels in components in the vicinity of the detectors.

A similar large-scale Ge effort is being pursued for the CDEX-300 ν experiment [52]. Like GERDA and LEGEND, the detectors will be immersed in liquid argon that serves as both a cooling medium and veto detector. CDEX-300 ν is expected to demonstrate a half-life sensitivity of $T_{\frac{1}{2}}^{0\nu} > 3.3 \times 10^{27}$ yr with an effective runtime of 10 years. Small prototypes with a detector mass of ~ 1 kg have been deployed.

(b) ^{136}Xe ($Q_{\beta\beta} = 2457.8$ keV)

The KamLAND-Zen [53] (Kamioka Liquid Scintillator Anti-Neutrino Detector Zero-Neutrino) series of experiments is located at the Kamioka Observatory, Japan. Its KamLAND-Zen 800 phase uses 745 kg of Xe gas, enriched to 90-91% and dissolved at 3% by weight into liquid scintillator in a nylon inner balloon, which in turn is surrounded by 1 kilo-ton of liquid scintillator acting as an active shield. ^{214}Bi , cosmogenic spallation products such as ^{10}C , and $2\nu\beta\beta$ itself were found to be the dominant backgrounds for its predecessor KamLAND-Zen 400, which had about half of the enriched Xe mass. While KamLAND-Zen now has the best background index compared to all active and past experiments, it also has the worst detector resolution of experiments

mentioned here (Fig. 3). Nevertheless, KamLAND-Zen provides a world-leading ^{136}Xe limit of $T_{\frac{1}{2}}^{0\nu}$ (Table 1). KamLAND-Zen plans to upgrade to KamLAND2-Zen, where 1 ton of enriched Xe will be deployed with a much brighter liquid scintillator and photomultiplier tubes of higher quantum efficiency to improve the energy resolution by a factor of two. KamLAND2-Zen is projected to have a half-life sensitivity of $T_{\frac{1}{2}}^{0\nu} > 1.1 \times 10^{27}$ yr in 5 years.

The Enriched Xenon Observatory 200 (EXO-200) [54] was a liquid xenon (LXe), cylindrical time-projection chamber (TPC) located at the Waste Isolation Pilot Plant (WIPP) in Carlsbad, New Mexico, USA. The liquid-phase TPC provided good energy resolution and low background due to its ability to reconstruct event topology.

The next-generation Enriched Xenon Observatory (nEXO) [55], a successor to EXO-200, will also use an LXe TPC with approximately 5 tons of xenon enriched to 90% in ^{136}Xe . nEXO is projected to reach a half-life sensitivity of $T_{\frac{1}{2}}^{0\nu} > 1.35 \times 10^{28}$ yr with 10 years of data collection. nEXO aims to have an energy resolution of $<1\%$ (σ) in ROI and plans to reduce the EXO-200 background by a factor of ~ 1000 . The background projections for nEXO are based on its established radioassay data for most component materials and comprehensive particle tracking and event reconstruction simulations. The nEXO collaboration is currently exploring the feasibility of identifying and labelling the daughter atomic element Ba from the double-beta decay of ^{136}Xe . If this endeavour proves successful, it has the potential to significantly reduce nEXO's background to almost zero in its second phase.

The Neutrino Experiment with a Xenon TPC (NEXT) [74] located at Canfranc Underground Laboratory (LSC), Spain, will use high-pressure xenon-gas time-projection chambers. The experiment aims to capitalise on the naturally low fluctuations in the production of ionisation pairs in xenon gas – combined with electroluminescence to amplify the ionisation signal – resulting in an energy resolution of $<0.4\%$ (σ) at $Q_{\beta\beta}$. Moreover, the tracks left in gaseous xenon have distinct topological features for $0\nu\beta\beta$ events that can be used for background rejection. NEXT-White, a prototype for NEXT-100 and NEXT-1t, has recently successfully demonstrated the TPC technology with a small fiducial volume. NEXT-100 is currently under construction at LSC. NEXT-1t has an estimated half-life sensitivity of $>1 \times 10^{27}$ yr in less than 5 yr with ~ 1 ton of ^{136}Xe . NEXT also has its own programme exploring ways to tag the daughter Ba^{++} ions from ^{136}Xe decay.

(c) ^{130}Te ($Q_{\beta\beta} = 2527.5$ keV)

The Cryogenic Underground Observatory for Rare Events (CUORE) [56] is the first ton-scale experiment searching for $0\nu\beta\beta$ decay using low-temperature calorimeters. The detector, located at the LNGS, Italy, consists of an array of 988 $^{nat}\text{TeO}_2$ crystals; each crystal is equipped with an neutron-transmutation doped germanium (NTD-Ge) thermistor and operated at close to 10 mK. In 2021, CUORE released results corresponding to a ton-year of $^{nat}\text{TeO}_2$, the largest amount of data ever acquired with a solid-state detector. Low-temperature calorimeters have intrinsically low detector noise, and their detector resolution is comparable to semiconductor detectors. CUORE's background is dominated by the energy-degraded alpha events emanating from detector holders, giving it a high background index.

The SNO+ [57] experiment, located at the SNOLAB facility in Canada, will use ^{130}Te -loaded liquid scintillator. SNO+ developed a novel metal-loading technique using an organic scintillator that keeps the loading stable and enhances the light yield. The initial loading in SNO+ will be 0.5% ^{nat}Te by mass, providing a $T_{\frac{1}{2}}^{0\nu} > 2.1 \times 10^{26}$ yr after 3 years of data taking. The detector-related backgrounds have been measured in two data-taking phases using only water and only liquid scintillator. Deployment of Te-loaded scintillator is planned for 2024. Moreover, recent R&D efforts have shown that the ^{130}Te loading can be increased to 3% by mass with an acceptable scintillator light yield, which would significantly increase SNO+ sensitivity in the future.

(d) ^{100}Mo ($Q_{\beta\beta} = 3034.4$ keV)

The AMoRE [58] project aims to search for the neutrinoless double beta decay of ^{100}Mo using molybdate-based crystals as low-temperature calorimeters. It is located in the Yangyang Underground Laboratory (Y2L) in South Korea. The crystals use metallic magnetic calorimeters (MMCs) to read out phonon signals at milli-Kelvin temperatures. AMoRE-Pilot successfully demonstrated the technology. In 2021, the project moved on to the next phase AMoRE-I, which is currently running with a total of approximately 3 kg of ^{100}Mo mass. AMoRE-I is housed in the same cryostat used for AMoRE-Pilot. Preliminary results indicate a background rate of 4×10^{-2} counts/kg.keV.yr in the ROI, and a lower limit of $T_{\frac{1}{2}}^{0\nu} > 1.2 \times 10^{24}$ yr at 90% C.L. The next phase, AMoRE-II, is currently under preparation and will operate at Yemilab in South Korea. AMoRE-II will comprise approximately 400 molybdate crystals (~ 100 kg of ^{100}Mo), using both calcium molybdate (CMO) and lithium molybdate (LMO) crystals. The target sensitivity is $T_{\frac{1}{2}}^{0\nu} > 5 \times 10^{26}$ yr.

CUPID-Mo [59] was a demonstrator experiment that employed a dual readout of phonon and scintillating light signals to remove the α background, which is sensitivity-limiting for large-array, low-temperature calorimeter searches like CUORE. This effort followed the success of CUPID-0 [61], the first medium-scale experiment to discriminate α from γ/β backgrounds with scintillating crystals (Zn^{82}Se for CUPID-0). CUPID-Mo took data with 20 LMO crystals flanked by 20 auxiliary low-temperature germanium calorimeters that served as light detectors. Similar to CUORE, all the calorimeters were read out by NTD-Ge thermistors. CUPID-Mo achieved an α rejection efficiency of $>99.9\%$ and an energy resolution similar to the CUORE detectors. The high $Q_{\beta\beta}$, above most environmental γ lines, and its α rejection ability enabled CUPID-Mo to establish the feasibility of a larger LMO-based experiment.

CUORE Upgrade with Particle IDentification (CUPID) [60] is a next-generation, tonne-scale bolometric experiment that will combine the best of the cryogenic infrastructure developed for CUORE and the detector technology developed by CUPID-Mo. A total of 1596 LMO crystals will be installed inside the CUORE cryostat, for a total of 240 kg of ^{100}Mo . Each crystal will be flanked by two light detectors that will enable α rejection. In the baseline design, the estimated background is $<1 \times 10^{-4}$ counts/kg.keV.yr in the ROI, two orders of magnitude lower than CUORE with an energy resolution similar to CUPID-Mo. The projected half-life sensitivity is $T_{\frac{1}{2}}^{0\nu} > 1.4 \times 10^{27}$ yr at 90% C.L. for 10 years of livetime. In the future, CUPID aims to push the background index by another factor of 5 with additional purification of the crystals and nearby components, and by reducing the $2\nu\beta\beta$ pile-up background. Eventually, a new cryostat with much more radiopure materials could allow a push to the normal-ordering region. A large-scale infrastructure hosting CUPID-1T would also be uniquely positioned as a multi-isotope observatory, capable of simultaneously deploying multiple cryogenic calorimeters like Zn^{82}Se , $\text{Li}_2^{100}\text{MoO}_4$, $^{116}\text{CdWO}_4$, and $^{130}\text{TeO}_2$.

(e) Nuclear matrix elements (NMEs)

Knowledge of the NME for the light-neutrino exchange mechanism is one of the most crucial inputs needed for extracting $m_{\beta\beta}$ [75] from a measured decay rate. The NMEs are typically calculated using macroscopic many-body nuclear models like the proton-neutron quasiparticle random-phase approximation method, energy-density functional theory, and the interacting boson model or using microscopic models that employ realistic nuclear forces like those from the Nuclear Shell Model or *ab initio* methods. Refs. [41,76] survey each method with its strengths and weaknesses.

The microscopic models using *ab initio* methods are computationally complex and have been applied to only light and medium $\beta\beta$ emitters [77,78]. While macroscopic models have slightly less computational complexity and can cover a wide range of $\beta\beta$ nuclei, they rely on fitting model parameters to a set of experimental observables. The most frequently used nuclear-structure

models are the interacting-boson model, the quasiparticle random-phase approximation, energy-density-functional methods, the generator-coordinate method, and the nuclear shell model [41, 69]. One of the major concerns for nuclear models was the disagreement between the decay rates predicted for β -decay and $2\nu\beta\beta$ -decay, which could be resolved by adjusting g_A to a lower value from its nominal value. Since the decay rate for $0\nu\beta\beta$ has a quartic dependence on g_A , a reduced value would significantly affect the half-life sensitivity. However, Ref. [79] seems to have resolved the discrepancy by including previously neglected nuclear correlations using *ab initio* methods. For many-body theories, calculations continuously improve as our comprehension of various nuclear interactions becomes more refined. Some of these interactions can enhance or suppress the values of the NMEs. For example, Ref. [80] shows that including two-body currents is a key ingredient for calculations and can suppress the $0\nu\beta\beta$ NMEs by $\sim 30\%$. On the other hand, recently introduced short-range $0\nu\beta\beta$ NMEs [81] may enhance the rate [82,83] by as much as $\sim 30\text{--}50\%$.

Given the complexity of the $0\nu\beta\beta$ decay process, one needs independent nuclear wavefunction tests to understand and characterise NMEs. There is no one suitable experimental probe that can cover the wide range of momentum components and multipolarities within the nuclear states involved – the Majorana-neutrino exchange between the two nucleons is localised within ~ 2 fm, resulting in a momentum spread of 105 MeV/ c [76]. Nevertheless, experimental data from various sources, including studies on ordinary muon capture [84,85], nucleon transfer reactions [86,87], double gamma decay [88], and reactions involving single-charge exchange (SCE) and double-charge exchange (DCE) [89], have been or can be utilised to constrain specific aspects of the calculations related to NMEs in $0\nu\beta\beta$ decay. A good correlation has also been found between the $2\nu\beta\beta$ and $0\nu\beta\beta$ decay NMEs [90,91]. However, in $2\nu\beta\beta$ -decay only the low-momentum (few MeV/ c) components of the nuclear wave functions are probed, and hence, they may not be enough to make deductions for the $0\nu\beta\beta$ -decay NMEs.

Recently, DCE reactions have received significant attention as probes for $0\nu\beta\beta$ -decay NMEs. They share the same initial and final states as $\beta\beta$ -decay, can probe a broad range of momentum and multipolarities in intermediate odd-odd isobar nuclei, and are sensitive to nucleon-nucleon interactions, thus resembling some aspects of the $0\nu\beta\beta$ -decay mechanism [92]. The NUMEN (NUclear Matrix Elements for Neutrinoless double beta decay) project aims to systematically investigate various Heavy-Ion-DCE reactions to extract essential information needed for NME calculation [93]. The experimental challenges for NUMEN are immense since the relevant cross sections are tiny (few tens of nano-barns), which requires high ion-beam intensities, with excellent particle identification to select the relevant nuclear channel, and high energy and angular resolution to resolve the transitions to different states from the energy spectra. Separate exploratory studies have been performed on different reactions in search of the most promising probe for DCE [94–96]. Several collaborations also aim to measure ordinary muon capture on double-beta decay-isotopes [85,97,98].

4. Additional intersections of neutrino and nuclear physics

(a) Nuclear physics for high-energy neutrino scattering

Accelerator neutrino beams with energies of order $0.1\text{--}10$ GeV are used to explore fundamental mysteries of neutrino physics ranging from the ordering of the neutrino-mass values, the unitarity of the PMNS mixing matrix, and the presence and scale of any CP violation in the neutrino sector. The upcoming, large-scale, long-baseline neutrino experiments Hyper-Kamiokande [99] (producing neutrinos at J-PARC and observing them at the Kamioka Observatory, Japan) and the Deep Underground Neutrino Experiment (DUNE, producing neutrinos at Fermilab and observing them at SURF, USA) [100] rely on such beams. Nuclear physics enters these measurements both via the neutrino source, typically a decay-in-flight pion beam produced by protons striking a thin target, and via the observation of a neutrino interaction in a detector medium. Conventional neutrino beams are not monoenergetic, although the detector location

can be chosen to sample a particular region of the energy distribution. The neutrino energy E_ν must be reconstructed from the event data and is thus affected not only by the energy-dependent cross section but also by uncertainties in the modelling of the target nucleus, including resonant processes; hadronic final-state interactions within the nuclear medium; secondary interactions outside the nucleus; and the final-state topology [101].

Nuclear processes are now recognised as a major limiting factor on the sensitivity of large neutrino-oscillation experiments, e.g. [102,103]. In principle, they are included in the Monte-Carlo event generators that simulate neutrino-nucleus interactions [104]. However, the accuracy of these simulations is hindered by a lack of experimental data and precise theoretical calculations, driving substantial investment in both dedicated experiments and sophisticated near-the-source detectors that simultaneously normalise the flux for long-baseline experiments and pursue independent physics measurements. Indeed, standard event generators are discrepant with measured neutrino interactions, e.g. [105,106]. These discrepancies may point to insufficient constraints on the axial coupling to the nucleon as well as to nuclear effects [107]. Future neutrino-scattering measurements – whether via the near detectors of short- or long-baseline oscillation experiments, or via dedicated experiments such as ANNIE [108], NINJA [109], or nuSTORM [110] – will help illuminate these issues, although in these measurements it is challenging to disentangle the specific physics mechanisms underlying any discrepancies. Neutrino-nucleon scattering measurements on hydrogen or deuterium targets may help disambiguate results [111].

Pion-nucleus scattering measurements probe hadronic final-state interactions within the target nucleus. Recent and future experimental efforts in this line focus on the same targets used by current and next-generation neutrino detectors: water [112]; carbon [113,114]; and argon [115,116]. World π^\pm data is already being used to tune the NEUT intranuclear cascade model [117].

Electron-nucleus scattering measurements exploit both high statistics and precise control of incident electron energies and final-state kinematics to probe the vector part of lepton-nucleus interactions, as reviewed in Ref. [118]. A recent test of neutrino energy-reconstruction techniques against electron scattering data on ^4He , ^{12}C and ^{56}Fe revealed significant discrepancies [119]. Current [120,121] and planned [122] measurements explore nuclear spectral functions and lepton-nucleus cross sections. Extensions of neutrino event-generators to predict electron-scattering observables are underway, e.g. Ref. [123].

In addition to constraining the nuclear physics of neutrino interactions, neutrino-scattering experiments also probe core questions in nuclear physics. For example, MINERvA recently made the first direct measurement of the free-proton axial-vector form factor, based on an analysis of $\bar{\nu}_\mu + p \rightarrow \mu^+ + n$ events [124], and the planned DUNE near detector will measure the electroweak mixing angle $\sin^2 \theta_W$ and probe isospin physics in hydrocarbon and argon targets [125].

(b) Nuclear physics from low-energy neutrino scattering

At low energies, neutrino scattering becomes a probe of nuclear structure. Coherent elastic neutrino-nucleus scattering (CEvNS), a neutral-current interaction with a relatively large cross section, probes the neutron distribution within a nucleus [126]. The complete COHERENT data set on CsI [127] has been used to determine the averaged neutron radius R_n for Cs and I to within about 6%; the precision can be improved by combination with atomic parity-violation data [128]. Appropriate nuclear targets for CEvNS allow low detection thresholds; by contrast, nuclear targets for R_n via parity-violating electron scattering (^{27}Al [129], ^{48}Ca [130], ^{208}Pb [131]) are chosen for high-lying nuclear excited states and for robustness under intense irradiation. Both neutrino- and electron-scattering techniques avoid the model dependencies of hadronic probes [132] while illuminating complementary regions of the neutron-distribution landscape. Combined with measurements of the proton radius, these results explore the nuclear symmetry energy and inform our understanding of neutron stars [133].

Neutrinos with energy of order 10 MeV are an important driver of supernova nucleosynthesis, interacting with abundant nuclei in the collapsing star to produce rare, often neutron-poor isotopes [134,135]. Direct measurements of these charged-current interactions are useful inputs

to models of this ν -process nucleosynthesis. Supernova neutrinos of $\mathcal{O}(1 - 10)$ MeV will appear in worldwide detectors through a variety of detection channels [136], many of which will benefit from dedicated measurements to reduce uncertainties on supernova dynamics and other observables. Two recent charged-current measurements from COHERENT – $^{nat}\text{Pb}(\nu_e, Xn)$ [137] and $^{127}\text{I}(\nu_e, Xn)$ [138] – show significant deficits relative to theoretical predictions in the MARLEY framework [139], highlighting the need for further work.

(c) Reactor antineutrinos and nuclear physics

Nuclear reactors produce copious amounts of $\bar{\nu}_e$ via beta-decay chains fed by fission reactions in the core. The first experimental discovery of neutrinos was made at the Savannah River reactor [2]. Since then, reactor antineutrinos have been instrumental in completing the picture of three-neutrino oscillation. The large-scale Jiangmen Underground Neutrino Observatory (JUNO), under construction in China, will observe reactor antineutrinos [140].

In the last decade, high-precision reactor experiments independently observed two anomalies sometimes taken as evidence of sterile neutrinos: a $\sim 5 - 6\%$ flux deficit relative to the Huber-Muller prediction [141,142] based on the conversion of summed beta spectra to antineutrino spectra, and an excess of antineutrinos at about 5 MeV [143–145]. Extensive experimental and theoretical work, including new beta-spectrum measurements [146], a reconsideration of decay-heat measurements [147], and studies of the neutrino flux for different fuel compositions [148–150], suggest attribution of the flux deficit to biases in the model inputs. Meanwhile, investigations of the 5-MeV excess revealed errors in nuclear databases [151]; the precise origin of this feature remains unclear, but the likely presence of contributions from all primary fission isotopes suggests a common error in the flux prediction [152]. Precise reactor-antineutrino measurements are improving our understanding of nuclear fission.

The impossibility of shielding antineutrinos gives them an appealing possible application in nuclear non-proliferation, recently reviewed in Ref. [153]: in principle, measuring characteristic antineutrino spectra allows the detection of a covert fission plant, or non-invasive monitoring of spent fuel or reactor operations. However, neutrino detection (especially in a high-background reactor environment) requires both significant financial investment and exposure time, and is likely impractical without facility cooperation. The Nu Tools study, based on discussions with end users in nuclear energy and nuclear security, found that neutrino monitoring would most likely be useful in the context of future nuclear deals; assay of spent fuel in dry casks; and future advanced reactors where traditional accountancy methods cannot be used [154]. Further development is needed for practical neutrino monitoring.

(d) Searching for sterile neutrinos with nuclear physics

Apart from reactor-based searches (Sec. (c)), nuclear physics is key to non-oscillation-based searches for sterile neutrinos. The spectrum from a beta or electron-capture decay (Sec. 2) is, in principle, a superposition of spectra: one for each neutrino-mass state, the mass value of which shifts the endpoint of the spectrum. Although the splittings of the three known mass states are too small for current-generation measurements to resolve, the presence of a fourth, widely separated neutrino-mass value m_4 will generate a kink-like spectral distortion at $E_0 - m_4$, where E_0 is the spectral endpoint. KATRIN has searched for this sterile-neutrino signature at both the eV scale [156], excluding significant portions of the parameter space that could explain the reactor flux deficit, and (using a commissioning data set) at the keV scale [157]. A planned future phase of KATRIN will perform higher-sensitivity searches for keV-scale sterile neutrinos with high-rate, deep spectral measurements enabled by the TRISTAN detector upgrade [15]. Planned Project 8 operations would further improve sensitivity at the eV scale [158].

Neutrino-mass experiments favour low E_0 , setting a ceiling on any observable value of m_4 . Two experiments aim to push past that ceiling by precisely measuring the kinematics of electron-capture decays with higher E_0 : ^7Be (BeEST, first limit set in Ref. [159]) and ^{131}Cs

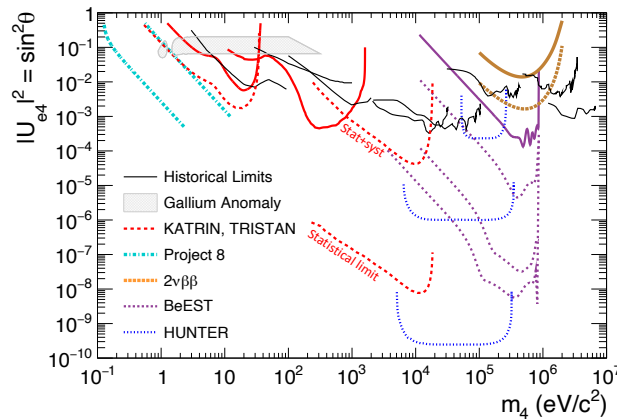


Figure 4. Achieved (solid) and projected (dotted) exclusion curves for sterile neutrinos from β -decay experiments, along with the parameter space preferred by the gallium anomaly (2σ contours). Adapted from Ref. [155].

(HUNTER, planned [160]). This allows kinematic reconstruction of the neutrino four-momentum and corresponding sensitivity to a heavy mass state. The presence of a sterile neutrino would also affect the electron kinematics in $2\nu\beta\beta$ decay; Bolton et al. [161] explore the corresponding sensitivity of $0\nu\beta\beta$ -decay searches (Sec. 3) to sterile neutrinos. Fig. 4 shows the existing (solid) and projected (dotted) limits on sterile-neutrino mixing $|U_{e4}|^2$ and mass m_4 from beta-decay and double-beta-decay experiments.

Beyond beta decays, nuclear physics may also be central to the longstanding gallium anomaly. When a high-intensity ν_e source irradiates a gallium target, $^{71}\text{Ga}(\nu_e, e^-)^{71}\text{Ge}$ interactions may be counted using radiochemical methods. The combined result of historical (GALLEX [162,163] and SAGE [164,165]) and modern (BEST [166]) experiments is a significant deficit in the observed ν_e rate. An overestimation of the nuclear-interaction cross section has been proposed as an alternative explanation to the oscillation of ν_e into a sterile flavour; however, a recent recalculation of corrections to the cross section shows only modest effects, and the well-measured ground-state transition prohibits large changes [167]. Followup experiments with intense ν_e and $\bar{\nu}_e$ sources, or the realisation of a fundamental problem with the nuclear-interaction calculation, could help resolve this anomaly.

(e) Synergy between neutrino-nuclear physics and quantum sensing

Quantum sensing, broadly used to describe the use of quantum objects or phenomena for measuring physical quantities, whether classical or quantum, is playing a crucial role in advancing precision measurements and gaining prominence in cutting-edge neutrino-nuclear experiments. Transition-edge sensors (TES) are used to achieve precise energy spectra from nuclear- β decay (as seen in HOLMES [29]); explore coherent neutrino nuclear scattering (NUCLEUS [168] and RICOCHET [169]); and pursue next-generation $0\nu\beta\beta$ searches like CUPID [170]. Simultaneously, superconducting tunnel junctions (STJs) are instrumental in BeEST's [159] investigation of phenomena such as sterile-neutrino states, while ECHO [16] and AMoRE [58] are developing arrays of metallic magnetic calorimeters (MMCs) for a neutrino-mass measurement and a $0\nu\beta\beta$ -decay search, respectively. Project 8 [23] aims to develop superconducting parametric amplifiers near the quantum limit for a tritium-based m_β measurement, and the QTNM project [171] aims to push still further by adding quantum-sensor magnetometry. Experimental needs demand faster sensor response times, expanded channel capacity, and more efficient multiplexing capabilities to enable the simultaneous readout of multiple sensors on a single line. Cryogenic hardware employed for quantum-sensor readout predominantly relies on superconducting microwave resonators and superconducting quantum

interference devices (SQUIDS). These readout technologies have the potential for broader applications beyond quantum sensing, such as interfaces with large qubit arrays.

On the flip side, the development of low-radioactivity techniques, primarily designed to explore rare phenomena like $0\nu\beta\beta$ decays and dark-matter searches, offers a distinctive opportunity to address the impact of ionising radiation on quantum sensors for quantum computers that significantly rely on the quantum phenomena of coherence and entanglement. Recent works have explored low-radiation materials, shielding, and underground quantum-circuit locations to reduce the effect of ionising radiation on superconducting qubits [172, 173]. Ionising radiation can lead to correlated errors, which pose a significant challenge for error correction and jeopardise the performance of quantum algorithms [174–176]. Hence, understanding the physics of how ionising radiation thermalises in qubit devices is crucial for successful mitigation and for advancing quantum error correction at scale. While operating quantum computers deep underground, with extensive shielding material around them, may not be feasible for large-scale applications, deep underground nuclear-physics facilities present a unique opportunity to research radiation effects within a controlled environment.

5. Conclusion

Since 1930, when Pauli postulated the neutrino's existence to restore energy-momentum conservation in nuclear beta decays, we have learned a great deal about this ghostly particle. The 1956 discovery of neutrinos via inverse beta decay at a nuclear fission plant was a triumph of experimental neutrino physics. However, fundamental questions about neutrinos remain open despite significant theoretical and experimental progress. In this paper, we have reviewed the many connections between nuclear physics and neutrino physics, which illuminate questions in both areas.

In the Standard Model, the neutrinos are the only massless fermions. We now know that neutrinos in fact have mass, and we have seen how current and future beta-decay and electron-capture experiments can probe the neutrino mass scale below the current limit via direct kinematic measurements in various nuclei.

Although we have observed the second-order $2\nu\beta\beta$ decay in certain nuclei, we have yet to detect lepton-number-violating $0\nu\beta\beta$ decay in any nucleus. We have discussed future experiments with ever larger sizes and higher sensitivities that will investigate the possibility that neutrinos are their own antiparticles (i.e., whether they are Majorana fermions).

Finally, we discuss additional ways in which nuclear physics and neutrino physics intertwine, from final states in high-energy interactions, to nuclear structure, to searches for sterile neutrinos, to cutting-edge developments in quantum sensing. The quest to understand neutrino properties is a multi-disciplinary effort, and the nucleus is a critical laboratory for many of these endeavours.

Acknowledgements. DSP acknowledges support from the U.S. Department of Energy (DOE), Office of Science, under Award Numbers DE-SC0010118, DE-SC0019304 and DE-SC0022125. AP is supported by the U.S. DOE under Federal Prime Agreement DE-AC02-05CH11231. VS is supported by the U.S. DOE, Office of Science, under grant DE-FG02-00ER41138. We thank Alexey Lokhov, Moritz Machatschek, Lisa Schlüter, Pranava Teja Surukuchi, and Kathrin Valerius for their useful contributions and suggestions.

References

1. Pauli W. 1930 Liebe Radioaktive Damen und Herren. Letter to conference attendees in Tübingen.
2. Cowan CL, Reines F, Harrison FB, Kruse HW, McGuire AD. 1956 Detection of the free neutrino: A Confirmation. *Science* **124**, 103–104. ([10.1126/science.124.3212.103](https://doi.org/10.1126/science.124.3212.103))
3. Gann GDO, Zuber K, Bemmerer D, Serenelli A. 2021 The Future of Solar Neutrinos. *Ann. Rev. Nucl. Part. Sci.* **71**, 491–528. ([10.1146/annurev-nucl-011921-061243](https://doi.org/10.1146/annurev-nucl-011921-061243))
4. Workman RL et al.. 2022 Review of Particle Physics. *PTEP* **2022**, 083C01. ([10.1093/ptep/ptac097](https://doi.org/10.1093/ptep/ptac097))

5. Fukuda Y et al.. 1998 Evidence for oscillation of atmospheric neutrinos. *Phys. Rev. Lett.* **81**, 1562–1567. ([10.1103/PhysRevLett.81.1562](https://doi.org/10.1103/PhysRevLett.81.1562))
6. Ahmad QR et al.. 2002 Direct evidence for neutrino flavor transformation from neutral current interactions in the Sudbury Neutrino Observatory. *Phys. Rev. Lett.* **89**, 011301. ([10.1103/PhysRevLett.89.011301](https://doi.org/10.1103/PhysRevLett.89.011301))
7. Eguchi K et al.. 2003 First results from KamLAND: Evidence for reactor anti-neutrino disappearance. *Phys. Rev. Lett.* **90**, 021802. ([10.1103/PhysRevLett.90.021802](https://doi.org/10.1103/PhysRevLett.90.021802))
8. Fermi E. 1934 Versuch einer Theorie der β -Strahlen. I. *Zeitschrift für Physik* **88**, 161–177. ([10.1007/BF01351864](https://doi.org/10.1007/BF01351864))
9. Formaggio JA, de Gouvêa ALC, Robertson RGH. 2021 Direct Measurements of Neutrino Mass. *Phys. Rept.* **914**, 1–54. ([10.1016/j.physrep.2021.02.002](https://doi.org/10.1016/j.physrep.2021.02.002))
10. Keblbeck DK, Bhandari R, Gamage ND, Gamage MH, Leach KG, Mougeot X, Redshaw M. 2023 Updated evaluation of potential ultralow Q-value β -decay candidates. *Phys. Rev. C* **107**, 015504. ([10.1103/PhysRevC.107.015504](https://doi.org/10.1103/PhysRevC.107.015504))
11. Kleesiek M et al.. 2019 β -Decay Spectrum, Response Function and Statistical Model for Neutrino Mass Measurements with the KATRIN Experiment. *Eur. Phys. J. C* **79**, 204. ([10.1140/epjc/s10052-019-6686-7](https://doi.org/10.1140/epjc/s10052-019-6686-7))
12. Aker M et al.. 2021 The design, construction, and commissioning of the KATRIN experiment. *JINST* **16**, T08015. ([10.1088/1748-0221/16/08/T08015](https://doi.org/10.1088/1748-0221/16/08/T08015))
13. Aker M et al.. 2022 Direct neutrino-mass measurement with sub-electronvolt sensitivity. *Nature Phys.* **18**, 160–166. ([10.1038/s41567-021-01463-1](https://doi.org/10.1038/s41567-021-01463-1))
14. Otten EW, Weinheimer C. 2008 Neutrino mass limit from tritium beta decay. *Rept. Prog. Phys.* **71**, 086201. ([10.1088/0034-4885/71/8/086201](https://doi.org/10.1088/0034-4885/71/8/086201))
15. Aker M et al.. 2022 KATRIN: status and prospects for the neutrino mass and beyond. *J. Phys. G* **49**, 100501. ([10.1088/1361-6471/ac834e](https://doi.org/10.1088/1361-6471/ac834e))
16. Velte C et al.. 2019 High-resolution and low-background ^{163}Ho spectrum: interpretation of the resonance tails. *Eur. Phys. J. C* **79**, 1026. ([10.1140/epjc/s10052-019-7513-x](https://doi.org/10.1140/epjc/s10052-019-7513-x))
17. Robertson RGH, Knapp DA. 1988 Direct Measurements of Neutrino Mass. *Ann. Rev. Nucl. Part. Sci.* **38**, 185–215. ([10.1146/annurev.ns.38.120188.001153](https://doi.org/10.1146/annurev.ns.38.120188.001153))
18. Saenz A, Jonsell S, Froelich P. 2000 Improved Molecular Final-State Distribution of HeT+ for the β -Decay Process of T2. *Phys. Rev. Lett.* **84**, 242. ([10.1103/PhysRevLett.84.242](https://doi.org/10.1103/PhysRevLett.84.242))
19. Bodine LI, Parno DS, Robertson RGH. 2015 Assessment of molecular effects on neutrino mass measurements from tritium β decay. *Phys. Rev. C* **91**, 035505. ([10.1103/PhysRevC.91.035505](https://doi.org/10.1103/PhysRevC.91.035505))
20. Lin YT et al.. 2020 Beta decay of molecular tritium. *Phys. Rev. Lett.* **124**, 222502. ([10.1103/PhysRevLett.124.222502](https://doi.org/10.1103/PhysRevLett.124.222502))
21. Monreal B, Formaggio JA. 2009 Relativistic Cyclotron Radiation Detection of Tritium Decay Electrons as a New Technique for Measuring the Neutrino Mass. *Phys. Rev. D* **80**, 051301. ([10.1103/PhysRevD.80.051301](https://doi.org/10.1103/PhysRevD.80.051301))
22. Asner DM et al.. 2015 Single electron detection and spectroscopy via relativistic cyclotron radiation. *Phys. Rev. Lett.* **114**, 162501. ([10.1103/PhysRevLett.114.162501](https://doi.org/10.1103/PhysRevLett.114.162501))
23. Ashtari Esfahani A et al.. 2023a Tritium Beta Spectrum Measurement and Neutrino Mass Limit from Cyclotron Radiation Emission Spectroscopy. *Phys. Rev. Lett.* **131**, 102502. ([10.1103/PhysRevLett.131.102502](https://doi.org/10.1103/PhysRevLett.131.102502))
24. Ashtari Esfahani A et al.. 2023b Cyclotron Radiation Emission Spectroscopy of Electrons from Tritium Beta Decay and $^{83\text{m}}\text{Kr}$ Internal Conversion. ([10.48550/arXiv.2303.12055](https://doi.org/10.48550/arXiv.2303.12055))
25. De Rujula A, Lusignoli M. 1982 Calorimetric Measurements of ^{163}Ho Decay as Tools to Determine the Electron Neutrino Mass. *Phys. Lett. B* **118**, 429. ([10.1016/0370-2693\(82\)90218-0](https://doi.org/10.1016/0370-2693(82)90218-0))
26. Nucciotti A. 2016 The use of low temperature detectors for direct measurements of the mass of the electron neutrino. *Adv. High Energy Phys.* **2016**, 9153024. ([10.1155/2016/9153024](https://doi.org/10.1155/2016/9153024))
27. Eliseev S et al.. 2015 Direct Measurement of the Mass Difference of ^{163}Ho and ^{163}Dy Solves the Q-Value Puzzle for the Neutrino Mass Determination. *Phys. Rev. Lett.* **115**, 062501. ([10.1103/PhysRevLett.115.062501](https://doi.org/10.1103/PhysRevLett.115.062501))
28. Braß M, Haverkort MW. 2020 *Abinitio* calculation of the electron capture spectrum of ^{163}Ho : Auger–Meitner decay into continuum states. *New J. Phys.* **22**, 093018. ([10.1088/1367-2630/abac72](https://doi.org/10.1088/1367-2630/abac72))
29. Giachero A et al.. 2017 Measuring the electron neutrino mass with improved sensitivity: the HOLMES experiment. *JINST* **12**, C02046. ([10.1088/1748-0221/12/02/C02046](https://doi.org/10.1088/1748-0221/12/02/C02046))
30. Griedel M et al.. 2022 From ECHo-1k to ECHo-100k: Optimization of High-Resolution Metallic

- Magnetic Calorimeters with Embedded ^{163}Ho for Neutrino Mass Determination. *J. Low Temp. Phys.* **209**, 779–787. ([10.1007/s10909-022-02732-w](https://doi.org/10.1007/s10909-022-02732-w))
31. Ullom J et al.. 2022 Measuring the electron neutrino mass using the electron capture decay of ^{163}Ho . In *Snowmass 2021*.
 32. Majorana E, Maiani L A symmetric theory of electrons and positrons. In *Ettore Majorana Scientific Papers: On occasion of the centenary of his birth*, pp. 201–233. Springer. ([10.1007/978-3-540-48095-2_10](https://doi.org/10.1007/978-3-540-48095-2_10))
 33. Fukugita M, Yanagida T. 1986 Baryogenesis Without Grand Unification. *Phys. Lett. B* **174**, 45–47. ([10.1016/0370-2693\(86\)91126-3](https://doi.org/10.1016/0370-2693(86)91126-3))
 34. Kotila J, Iachello F. 2012 Phase space factors for double- β decay. *Phys. Rev. C* **85**, 034316. ([10.1103/PhysRevC.85.034316](https://doi.org/10.1103/PhysRevC.85.034316))
 35. Deppisch FF, Graf L, Iachello F, Kotila J. 2020 Analysis of light neutrino exchange and short-range mechanisms in $0\nu\beta\beta$ decay. *Phys. Rev. D* **102**, 095016. ([10.1103/PhysRevD.102.095016](https://doi.org/10.1103/PhysRevD.102.095016))
 36. Mount BJ, Redshaw M, Myers EG. 2010 Double-beta-decay Q values of ^{74}Se and ^{76}Ge . *Phys. Rev. C* **81**, 032501. ([10.1103/PhysRevC.81.032501](https://doi.org/10.1103/PhysRevC.81.032501))
 37. Rahaman S et al.. 2008 Q values of the ^{76}Ge and ^{100}Mo double-beta decays. *Phys. Lett. B* **662**, 111–116. ([10.1016/j.physletb.2008.02.047](https://doi.org/10.1016/j.physletb.2008.02.047))
 38. Fink D et al.. 2012 Q-Value and Half-Lives for the Double-Beta-Decay Nuclide ^{110}Pd . *Phys. Rev. Lett.* **108**, 062502. ([10.1103/PhysRevLett.108.062502](https://doi.org/10.1103/PhysRevLett.108.062502))
 39. Scielzo ND et al.. 2009 Double-beta decay Q values of ^{130}Te , ^{128}Te , and ^{120}Te . *Phys. Rev. C* **80**, 025501. ([10.1103/PhysRevC.80.025501](https://doi.org/10.1103/PhysRevC.80.025501))
 40. Dolinski MJ, Poon AWP, Rodejohann W. 2019 Neutrinoless Double-Beta Decay: Status and Prospects. *Ann. Rev. Nucl. Part. Sci.* **69**, 219–251. ([10.1146/annurev-nucl-101918-023407](https://doi.org/10.1146/annurev-nucl-101918-023407))
 41. Engel J, Menéndez J. 2017 Status and Future of Nuclear Matrix Elements for Neutrinoless Double-Beta Decay: A Review. *Rept. Prog. Phys.* **80**, 046301. ([10.1088/1361-6633/aa5bc5](https://doi.org/10.1088/1361-6633/aa5bc5))
 42. Šimkovic F. 2021 Neutrino masses and interactions and neutrino experiments in the laboratory. *Usp. Fiz. Nauk* **191**, 1307–1332. ([10.3367/UFNe.2021.08.039036](https://doi.org/10.3367/UFNe.2021.08.039036))
 43. Schechter J, Valle JWF. 1982 Neutrinoless Double beta Decay in $\text{SU}(2) \times \text{U}(1)$ Theories. *Phys. Rev. D* **25**, 2951. ([10.1103/PhysRevD.25.2951](https://doi.org/10.1103/PhysRevD.25.2951))
 44. Nieves JF. 1984 Dirac and Pseudodirac Neutrinos and Neutrinoless Double Beta Decay. *Phys. Lett. B* **147**, 375–379. ([10.1016/0370-2693\(84\)90136-9](https://doi.org/10.1016/0370-2693(84)90136-9))
 45. Takasugi E. 1984 Can the Neutrinoless Double Beta Decay Take Place in the Case of Dirac Neutrinos?. *Phys. Lett. B* **149**, 372–376. ([10.1016/0370-2693\(84\)90426-X](https://doi.org/10.1016/0370-2693(84)90426-X))
 46. Moe MK. 1991 Experimental review of double beta decay. *Nucl. Phys. B Proc. Suppl.* **19**, 158–176. ([10.1016/0920-5632\(91\)90198-N](https://doi.org/10.1016/0920-5632(91)90198-N))
 47. Formaggio JA, Martoff CJ. 2004 Backgrounds to sensitive experiments underground. *Ann. Rev. Nucl. Part. Sci.* **54**, 361–412. ([10.1146/annurev.nucl.54.070103.181248](https://doi.org/10.1146/annurev.nucl.54.070103.181248))
 48. Ianni A. 2017 Review of technical features in underground laboratories. *Int. J. Mod. Phys. A* **32**, 1743001. ([10.1142/S0217751X17430011](https://doi.org/10.1142/S0217751X17430011))
 49. Agostini M et al.. 2020 Final Results of GERDA on the Search for Neutrinoless Double- β Decay. *Phys. Rev. Lett.* **125**, 252502. ([10.1103/PhysRevLett.125.252502](https://doi.org/10.1103/PhysRevLett.125.252502))
 50. Arnquist IJ et al.. 2023 Final Result of the Majorana Demonstrator’s Search for Neutrinoless Double- β Decay in Ge76 . *Phys. Rev. Lett.* **130**, 062501. ([10.1103/PhysRevLett.130.062501](https://doi.org/10.1103/PhysRevLett.130.062501))
 51. Abgrall N et al.. 2021 The Large Enriched Germanium Experiment for Neutrinoless $\beta\beta$ Decay: LEGEND-1000 Preconceptual Design Report. ([10.48550/arXiv.2107.11462](https://doi.org/10.48550/arXiv.2107.11462))
 52. Zhang BT et al.. 2023 Searching for ^{76}Ge neutrinoless double beta decay with the CDEX-1B experiment. ([10.48550/arXiv.2305.00894](https://doi.org/10.48550/arXiv.2305.00894))
 53. Abe S et al.. 2023 Search for the Majorana Nature of Neutrinos in the Inverted Mass Ordering Region with KamLAND-Zen. *Phys. Rev. Lett.* **130**, 051801. ([10.1103/PhysRevLett.130.051801](https://doi.org/10.1103/PhysRevLett.130.051801))
 54. Anton G et al.. 2019 Search for Neutrinoless Double- β Decay with the Complete EXO-200 Dataset. *Phys. Rev. Lett.* **123**, 161802. ([10.1103/PhysRevLett.123.161802](https://doi.org/10.1103/PhysRevLett.123.161802))
 55. Adhikari G et al.. 2022 nEXO: neutrinoless double beta decay search beyond 10^{28} year half-life sensitivity. *J. Phys. G* **49**, 015104. ([10.1088/1361-6471/ac3631](https://doi.org/10.1088/1361-6471/ac3631))
 56. Adams DQ et al.. 2022 Search for Majorana neutrinos exploiting millikelvin cryogenics with CUORE. *Nature* **604**, 53–58. ([10.1038/s41586-022-04497-4](https://doi.org/10.1038/s41586-022-04497-4))
 57. Chen MC. 2021 SNO+. *J. Phys. Conf. Ser.* **2156**, 012143. ([10.1088/1742-6596/2156/1/012143](https://doi.org/10.1088/1742-6596/2156/1/012143))
 58. Kim HB et al.. 2022 Status and Performance of the AMoRE-I Experiment on Neutrinoless Double Beta Decay. *J. Low Temp. Phys.* **209**, 962–970. ([10.1007/s10909-022-02880-z](https://doi.org/10.1007/s10909-022-02880-z))

59. Augier C et al.. 2022 Final results on the $0\nu\beta\beta$ decay half-life limit of ^{100}Mo from the CUPID-Mo experiment. *Eur. Phys. J. C* **82**, 1033. ([10.1140/epjc/s10052-022-10942-5](https://doi.org/10.1140/epjc/s10052-022-10942-5))
60. Armstrong WR et al.. 2019 CUPID pre-CDR. ([10.48550/arXiv.1907.09376](https://arxiv.org/abs/10.48550/arXiv.1907.09376))
61. Azzolini O et al.. 2022 Final Result on the Neutrinoless Double Beta Decay of ^{82}Se with CUPID-0. *Phys. Rev. Lett.* **129**, 111801. ([10.1103/PhysRevLett.129.111801](https://doi.org/10.1103/PhysRevLett.129.111801))
62. Quinn W. 2023 *The sensitivity of the NEMO technique to neutrinoless double beta decay and the commissioning of the SuperNEMO demonstrator module*. PhD thesis University Coll. London.
63. Ajimura S et al.. 2021 Low background measurement in CANDLES-III for studying the neutrino-less double beta decay of ^{48}Ca . *Phys. Rev. D* **103**, 092008. ([10.1103/PhysRevD.103.092008](https://doi.org/10.1103/PhysRevD.103.092008))
64. Agostini M, Benato G, Detwiler JA, Menéndez J, Vissani F. 2021 Testing the inverted neutrino mass ordering with neutrinoless double- β decay. *Phys. Rev. C* **104**, L042501. ([10.1103/PhysRevC.104.L042501](https://doi.org/10.1103/PhysRevC.104.L042501))
65. Deppisch F, Pas H. 2007 Pinning down the mechanism of neutrinoless double beta decay with measurements in different nuclei. *Phys. Rev. Lett.* **98**, 232501. ([10.1103/PhysRevLett.98.232501](https://doi.org/10.1103/PhysRevLett.98.232501))
66. Bossio E, Agostini M. 2023 Probing Beyond the Standard Model Physics with Double-beta Decays. ([10.48550/arXiv.2304.07198](https://arxiv.org/abs/10.48550/arXiv.2304.07198))
67. Lisi E, Marrone A, Nath N. 2023 Interplay between noninterfering neutrino exchange mechanisms and nuclear matrix elements in $0\nu\beta\beta$ decay. *Phys. Rev. D* **108**, 055023. ([10.1103/PhysRevD.108.055023](https://doi.org/10.1103/PhysRevD.108.055023))
68. Gráf L, Lindner M, Scholer O. 2022 Unraveling the $0\nu\beta\beta$ decay mechanisms. *Phys. Rev. D* **106**, 035022. ([10.1103/PhysRevD.106.035022](https://doi.org/10.1103/PhysRevD.106.035022))
69. Agostini M, Benato G, Detwiler JA, Menéndez J, Vissani F. 2023 Toward the discovery of matter creation with neutrinoless $\beta\beta$ decay. *Rev. Mod. Phys.* **95**, 025002. ([10.1103/RevModPhys.95.025002](https://doi.org/10.1103/RevModPhys.95.025002))
70. Dell’Oro S, Marcocci S, Viel M, Vissani F. 2016 Neutrinoless double beta decay: 2015 review. *Adv. High Energy Phys.* **2016**, 2162659. ([10.1155/2016/2162659](https://doi.org/10.1155/2016/2162659))
71. Vergados JD, Ejiri H, Simkovic F. 2012 Theory of Neutrinoless Double Beta Decay. *Rept. Prog. Phys.* **75**, 106301. ([10.1088/0034-4885/75/10/106301](https://doi.org/10.1088/0034-4885/75/10/106301))
72. Avignone, III FT, Elliott SR, Engel J. 2008 Double Beta Decay, Majorana Neutrinos, and Neutrino Mass. *Rev. Mod. Phys.* **80**, 481–516. ([10.1103/RevModPhys.80.481](https://doi.org/10.1103/RevModPhys.80.481))
73. Elliott SR, Vogel P. 2002 Double beta decay. *Ann. Rev. Nucl. Part. Sci.* **52**, 115–151. ([10.1146/annurev.nucl.52.050102.090641](https://doi.org/10.1146/annurev.nucl.52.050102.090641))
74. Adams C et al.. 2021 Sensitivity of a tonne-scale NEXT detector for neutrinoless double beta decay searches. *JHEP* **2021**, 164. ([10.1007/JHEP08\(2021\)164](https://doi.org/10.1007/JHEP08(2021)164))
75. Pompa F, Schwetz T, Zhu JY. 2023 Impact of nuclear matrix element calculations for current and future neutrinoless double beta decay searches. *JHEP* **06**, 104. ([10.1007/JHEP06\(2023\)104](https://doi.org/10.1007/JHEP06(2023)104))
76. Ejiri H, Suhonen J, Zuber K. 2019 Neutrino–nuclear responses for astro-neutrinos, single beta decays and double beta decays. *Phys. Rept.* **797**, 1–102. ([10.1016/j.physrep.2018.12.001](https://doi.org/10.1016/j.physrep.2018.12.001))
77. Yao JM, Bally B, Engel J, Wirth R, Rodríguez TR, Hergert H. 2020 *AbInitio* Treatment of Collective Correlations and the Neutrinoless Double Beta Decay of ^{48}Ca . *Phys. Rev. Lett.* **124**, 232501. ([10.1103/PhysRevLett.124.232501](https://doi.org/10.1103/PhysRevLett.124.232501))
78. Belley A, Payne CG, Stroberg SR, Miyagi T, Holt JD. 2021 *AbInitio* Neutrinoless Double-Beta Decay Matrix Elements for ^{48}Ca , ^{76}Ge , and ^{82}Se . *Phys. Rev. Lett.* **126**, 042502. ([10.1103/PhysRevLett.126.042502](https://doi.org/10.1103/PhysRevLett.126.042502))
79. Gysbers P et al.. 2019 Discrepancy between experimental and theoretical β -decay rates resolved from first principles. *Nature Phys.* **15**, 428–431. ([10.1038/s41567-019-0450-7](https://doi.org/10.1038/s41567-019-0450-7))
80. Menendez J, Gazit D, Schwenk A. 2011 Chiral two-body currents in nuclei: Gamow-Teller transitions and neutrinoless double-beta decay. *Phys. Rev. Lett.* **107**, 062501. ([10.1103/PhysRevLett.107.062501](https://doi.org/10.1103/PhysRevLett.107.062501))
81. Cirigliano V, Dekens W, De Vries J, Graesser ML, Mereghetti E, Pastore S, Piarulli M, Van Kolck U, Wiringa RB. 2019 Renormalized approach to neutrinoless double- β decay. *Phys. Rev. C* **100**, 055504. ([10.1103/PhysRevC.100.055504](https://doi.org/10.1103/PhysRevC.100.055504))
82. Wirth R, Yao JM, Hergert H. 2021 *Ab Initio* Calculation of the Contact Operator Contribution in the Standard Mechanism for Neutrinoless Double Beta Decay. *Phys. Rev. Lett.* **127**, 242502. ([10.1103/PhysRevLett.127.242502](https://doi.org/10.1103/PhysRevLett.127.242502))
83. Jokiniemi L, Soriano P, Menéndez J. 2021 Impact of the leading-order short-range nuclear matrix element on the neutrinoless double-beta decay of medium-mass and heavy nuclei. *Phys. Lett. B* **823**, 136720. ([10.1016/j.physletb.2021.136720](https://doi.org/10.1016/j.physletb.2021.136720))

84. Jokiniemi L, Suhonen J. 2020 Comparative analysis of muon-capture and $0\nu\beta\beta$ -decay matrix elements. *Phys. Rev. C* **102**, 024303. ([10.1103/PhysRevC.102.024303](https://doi.org/10.1103/PhysRevC.102.024303))
85. Hashim IH, Ejiri H. 2021 Ordinary Muon Capture for Double Beta Decay and Anti-Neutrino Nuclear Responses. *Front. Astron. Space Sci.* **8**, 82. ([10.3389/fspas.2021.666383](https://doi.org/10.3389/fspas.2021.666383))
86. Freeman SJ et al.. 2007 Pair correlations in nuclei involved in neutrinoless double beta decay: Ge-76 and Se-76. *Phys. Rev. C* **75**, 051301. ([10.1103/PhysRevC.75.051301](https://doi.org/10.1103/PhysRevC.75.051301))
87. Roberts A et al.. 2013 Proton pair correlations and the neutrinoless double- β decay of ^{76}Ge . *Phys. Rev. C* **87**, 051305. ([10.1103/PhysRevC.87.051305](https://doi.org/10.1103/PhysRevC.87.051305))
88. Romeo B, Menéndez J, Peña Garay C. 2022 $\gamma\gamma$ decay as a probe of neutrinoless $\beta\beta$ decay nuclear matrix elements. *Phys. Lett. B* **827**, 136965. ([10.1016/j.physletb.2022.136965](https://doi.org/10.1016/j.physletb.2022.136965))
89. Ejiri H. 2022 Single- and Double-Charge Exchange Reactions and Nuclear Matrix Element for Double-Beta Decay. *Universe* **8**, 457. ([10.3390/universe8090457](https://doi.org/10.3390/universe8090457))
90. Jokiniemi L, Romeo B, Soriano P, Menéndez J. 2023 Neutrinoless $\beta\beta$ -decay nuclear matrix elements from two-neutrino $\beta\beta$ -decay data. *Phys. Rev. C* **107**, 044305. ([10.1103/PhysRevC.107.044305](https://doi.org/10.1103/PhysRevC.107.044305))
91. Horoi M, Neacsu A, Stoica S. 2023 Predicting the neutrinoless double- β -decay matrix element of Xe136 using a statistical approach. *Phys. Rev. C* **107**, 045501. ([10.1103/PhysRevC.107.045501](https://doi.org/10.1103/PhysRevC.107.045501))
92. Cappuzzello F et al.. 2023 Shedding light on nuclear aspects of neutrinoless double beta decay by heavy-ion double charge exchange reactions. *Prog. Part. Nucl. Phys.* **128**, 103999. ([10.1016/j.pnpnp.2022.103999](https://doi.org/10.1016/j.pnpnp.2022.103999))
93. Cappuzzello F et al.. 2018 The NUMEN project: NUClear Matrix Elements for Neutrinoless double beta decay. *Eur. Phys. J. A* **54**, 72. ([10.1140/epja/i2018-12509-3](https://doi.org/10.1140/epja/i2018-12509-3))
94. Kisamori K et al.. 2016 Candidate Resonant Tetraneutron State Populated by the $^4\text{He}(^8\text{He}, ^8\text{Be})$ Reaction. *Phys. Rev. Lett.* **116**, 052501. ([10.1103/PhysRevLett.116.052501](https://doi.org/10.1103/PhysRevLett.116.052501))
95. Takahisa K, Ejiri H, Akimune H, Fujita H, Matsumiya R, Ohta T, Shima T, Tanaka M, Yoso M. 2017 Double charge exchange ($^{11}\text{B}, ^{11}\text{Li}$) reaction for double beta decay response. ([10.48550/arXiv.1703.08264](https://arxiv.org/abs/10.48550/arXiv.1703.08264))
96. Matsubara H et al.. 2013 Spectroscopic Measurement in ^9He and ^{12}Be . *Few Body Syst.* **54**, 1433–1436. ([10.1007/s00601-012-0586-9](https://doi.org/10.1007/s00601-012-0586-9))
97. Hashim IH et al.. 2023 Measurements of ordinary muon capture rates on Mo100 and natural Mo for astro-antineutrinos and double- β decays. *Phys. Rev. C* **108**, 014618. ([10.1103/PhysRevC.108.014618](https://doi.org/10.1103/PhysRevC.108.014618))
98. The MONUMENT collaboration, Contribution at the MEDEX'22 Workshop, Prague, Czech Republic. 13–17 June. 2022 The MONUMENT Experiment; Ordinary Muon Capture as a benchmark for $0\nu\beta\beta$ -decay nuclear structure calculations. <https://indico.utef.cvut.cz/event/32/contributions>.
99. Bian J et al.. 2022 Hyper-Kamiokande Experiment: A Snowmass White Paper. In *Snowmass 2021*. ([10.48550/arXiv.2203.02029](https://arxiv.org/abs/10.48550/arXiv.2203.02029))
100. Abed Abud A et al.. 2022 Snowmass Neutrino Frontier: DUNE Physics Summary. ([10.48550/arXiv.2203.06100](https://arxiv.org/abs/10.48550/arXiv.2203.06100))
101. Alvarez-Ruso L et al.. 2018 NuSTEC White Paper: Status and challenges of neutrino–nucleus scattering. *Prog. Part. Nucl. Phys.* **100**, 1–68. ([10.1016/j.pnpnp.2018.01.006](https://doi.org/10.1016/j.pnpnp.2018.01.006))
102. Benhar O, Huber P, Mariani C, Meloni D. 2017 Neutrino–nucleus interactions and the determination of oscillation parameters. *Phys. Rept.* **700**, 1–47. ([10.1016/j.physrep.2017.07.004](https://doi.org/10.1016/j.physrep.2017.07.004))
103. Balantekin AB et al.. 2022 Snowmass Neutrino Frontier: Neutrino Interaction Cross Sections (NF06) Topical Group Report. ([10.48550/arXiv.2209.06872](https://arxiv.org/abs/10.48550/arXiv.2209.06872))
104. Campbell JM et al.. 2022 Event Generators for High-Energy Physics Experiments. In *Snowmass 2021*. ([10.48550/arXiv.2203.11110](https://arxiv.org/abs/10.48550/arXiv.2203.11110))
105. Stowell P et al.. 2019 Tuning the GENIE Pion Production Model with MINER ν A Data. *Phys. Rev. D* **100**, 072005. ([10.1103/PhysRevD.100.072005](https://doi.org/10.1103/PhysRevD.100.072005))
106. Acero MA et al.. 2020 Adjusting neutrino interaction models and evaluating uncertainties using NO ν A near detector data. *Eur. Phys. J. C* **80**, 1119. ([10.1140/epjc/s10052-020-08577-5](https://doi.org/10.1140/epjc/s10052-020-08577-5))
107. Nikolakopoulos A, González-Jiménez R, Jachowicz N, Udías JM. 2023 Assessing the theory-data tension in neutrino-induced charged pion production: The effect of final-state nucleon distortion. *Phys. Rev. D* **107**, 053007. ([10.1103/PhysRevD.107.053007](https://doi.org/10.1103/PhysRevD.107.053007))
108. Back AR et al.. 2020 Measurement of Beam-Related Background Neutrons from the Fermilab Booster Neutrino Beam in ANNIE Phase-I. *JINST* **15**, P03011. ([10.1088/1748-0221/15/03/P03011](https://doi.org/10.1088/1748-0221/15/03/P03011))

109. Hiramoto A et al.. 2020 First measurement of $\bar{\nu}_\mu$ and ν_μ charged-current inclusive interactions on water using a nuclear emulsion detector. *Phys. Rev. D* **102**, 072006. ([10.1103/PhysRevD.102.072006](https://doi.org/10.1103/PhysRevD.102.072006))
110. Ruso LA et al.. 2022 Neutrinos from Stored Muons (nuSTORM). In *Snowmass 2021*. ([10.48550/arXiv.2203.07545](https://arxiv.org/abs/2203.07545))
111. Alvarez-Ruso L et al.. 2022 Neutrino Scattering Measurements on Hydrogen and Deuterium: A Snowmass White Paper. ([10.48550/arXiv.2203.11298](https://arxiv.org/abs/2203.11298))
112. Yamauchi K, Ishitsuka M, Shinoki M, Kuze M, Hartz M. 2021 Evaluation of event reconstruction with small-scale water Cherenkov detectors. *J. Phys. Conf. Ser.* **2156**, 012199. ([10.1088/1742-6596/2156/1/012199](https://doi.org/10.1088/1742-6596/2156/1/012199))
113. Ieki K et al.. 2015 Measurement of absorption and charge exchange of π^+ on carbon. *Phys. Rev. C* **92**, 035205. ([10.1103/PhysRevC.92.035205](https://doi.org/10.1103/PhysRevC.92.035205))
114. Pinzon Guerra ES et al.. 2017 Measurement of σ_{ABS} and σ_{CX} of π^+ on carbon by the Dual Use Experiment at TRIUMF (DUET). *Phys. Rev. C* **95**, 045203. ([10.1103/PhysRevC.95.045203](https://doi.org/10.1103/PhysRevC.95.045203))
115. Acciarri R et al.. 2020 The Liquid Argon In A Testbeam (LArLAT) Experiment. *JINST* **15**, P04026. ([10.1088/1748-0221/15/04/P04026](https://doi.org/10.1088/1748-0221/15/04/P04026))
116. Abud AA et al.. 2022 Design, construction and operation of the ProtoDUNE-SP Liquid Argon TPC. *JINST* **17**, P01005. ([10.1088/1748-0221/17/01/P01005](https://doi.org/10.1088/1748-0221/17/01/P01005))
117. Pinzon Guerra ES et al.. 2019 Using world charged π^\pm -nucleus scattering data to constrain an intranuclear cascade model. *Phys. Rev. D* **99**, 052007. ([10.1103/PhysRevD.99.052007](https://doi.org/10.1103/PhysRevD.99.052007))
118. Ankowski AM et al.. 2022 Electron Scattering and Neutrino Physics. ([10.48550/arXiv.2203.06853](https://arxiv.org/abs/2203.06853))
119. Khachatryan M et al.. 2021 Electron-beam energy reconstruction for neutrino oscillation measurements. *Nature* **599**, 565–570. ([10.1038/s41586-021-04046-5](https://doi.org/10.1038/s41586-021-04046-5))
120. Jiang L et al.. 2022 Determination of the argon spectral function from (e,e'p) data. *Phys. Rev. D* **105**, 112002. ([10.1103/PhysRevD.105.112002](https://doi.org/10.1103/PhysRevD.105.112002))
121. Jiang L et al.. 2023 Determination of the titanium spectral function from (e, e'p) data. *Phys. Rev. D* **107**, 012005. ([10.1103/PhysRevD.107.012005](https://doi.org/10.1103/PhysRevD.107.012005))
122. Ankowski AM, Friedland A, Li SW, Moreno O, Schuster P, Toro N, Tran N. 2020 Lepton-Nucleus Cross Section Measurements for DUNE with the LDMX Detector. *Phys. Rev. D* **101**, 053004. ([10.1103/PhysRevD.101.053004](https://doi.org/10.1103/PhysRevD.101.053004))
123. Papadopoulou A et al.. 2021 Inclusive Electron Scattering And The GENIE Neutrino Event Generator. *Phys. Rev. D* **103**, 113003. ([10.1103/PhysRevD.103.113003](https://doi.org/10.1103/PhysRevD.103.113003))
124. Cai T et al.. 2023 Measurement of the axial vector form factor from antineutrino-proton scattering. *Nature* **614**, 48–53. ([10.1038/s41586-022-05478-3](https://doi.org/10.1038/s41586-022-05478-3))
125. Hewes V et al.. 2021 Deep Underground Neutrino Experiment (DUNE) Near Detector Conceptual Design Report. *Instruments* **5**, 31. ([10.3390/instruments5040031](https://doi.org/10.3390/instruments5040031))
126. Abdullah M et al.. 2022 Coherent elastic neutrino-nucleus scattering: Terrestrial and astrophysical applications. ([10.48550/arXiv.2203.07361](https://arxiv.org/abs/2203.07361))
127. Akimov D et al.. 2022 Measurement of the Coherent Elastic Neutrino-Nucleus Scattering Cross Section on CsI by COHERENT. *Phys. Rev. Lett.* **129**, 081801. ([10.1103/PhysRevLett.129.081801](https://doi.org/10.1103/PhysRevLett.129.081801))
128. Atzori Corona M et al.. 2023 Nuclear neutron radius and weak mixing angle measurements from latest COHERENT CsI and atomic parity violation Cs data. ([10.48550/arXiv.2303.09360](https://arxiv.org/abs/2303.09360))
129. Androic D et al.. 2022 Determination of the ^{27}Al Neutron Distribution Radius from a Parity-Violating Electron Scattering Measurement. *Phys. Rev. Lett.* **128**, 132501. ([10.1103/PhysRevLett.128.132501](https://doi.org/10.1103/PhysRevLett.128.132501))
130. Adhikari D et al.. 2022 Precision Determination of the Neutral Weak Form Factor of ^{48}Ca . *Phys. Rev. Lett.* **129**, 042501. ([10.1103/PhysRevLett.129.042501](https://doi.org/10.1103/PhysRevLett.129.042501))
131. Adhikari D et al.. 2021 Accurate Determination of the Neutron Skin Thickness of ^{208}Pb through Parity-Violation in Electron Scattering. *Phys. Rev. Lett.* **126**, 172502. ([10.1103/PhysRevLett.126.172502](https://doi.org/10.1103/PhysRevLett.126.172502))
132. Thiel M, Sfienti C, Piekarewicz J, Horowitz CJ, Vanderhaeghen M. 2019 Neutron skins of atomic nuclei: per aspera ad astra. *J. Phys. G* **46**, 093003. ([10.1088/1361-6471/ab2c6d](https://doi.org/10.1088/1361-6471/ab2c6d))
133. Horowitz CJ, Pollock SJ, Souder PA, Michaels R. 2001 Parity violating measurements of neutron densities. *Phys. Rev. C* **63**, 025501. ([10.1103/PhysRevC.63.025501](https://doi.org/10.1103/PhysRevC.63.025501))
134. Woosley SE, Hartmann DH, Hoffman RD, Haxton WC. 1990 The ν -process. *Astrophys. J.* **356**, 272. ([10.1086/168839](https://doi.org/10.1086/168839))

135. Sieverding A, Martínez-Pinedo G, Langanke K, Bollig R, Janka HT, Heger A. 2019 The ν -process with Fully Time-dependent Supernova Neutrino Emission Spectra. *Astrophys. J.* **876**, 151. ([10.3847/1538-4357/ab17e2](https://doi.org/10.3847/1538-4357/ab17e2))
136. Scholberg K. 2012 Supernova Neutrino Detection. *Ann. Rev. Nucl. Part. Sci.* **62**, 81–103. ([10.1146/annurev-nucl-102711-095006](https://doi.org/10.1146/annurev-nucl-102711-095006))
137. An P et al.. 2022 Measurement of $^{nat}\text{Pb}(\nu_e, Xn)$ production with a stopped-pion neutrino source. ([10.48550/arXiv.2212.11295](https://arxiv.org/abs/10.48550/arXiv.2212.11295))
138. An P et al.. 2023 Measurement of the inclusive electron-neutrino charged-current cross section on ^{127}I with the COHERENT NaI ν E detector. ([10.48550/arXiv.2305.19594](https://arxiv.org/abs/10.48550/arXiv.2305.19594))
139. Gardiner S. 2021 Simulating low-energy neutrino interactions with MARLEY. *Comput. Phys. Commun.* **269**, 108123. ([10.1016/j.cpc.2021.108123](https://doi.org/10.1016/j.cpc.2021.108123))
140. Abusleme A et al.. 2022 JUNO physics and detector. *Prog. Part. Nucl. Phys.* **123**, 103927. ([10.1016/j.pnpnp.2021.103927](https://doi.org/10.1016/j.pnpnp.2021.103927))
141. Huber P. 2011 On the determination of anti-neutrino spectra from nuclear reactors. *Phys. Rev. C* **84**, 024617. [Erratum: *Phys. Rev. C* **85**, 029901 (2012)] ([10.1103/PhysRevC.85.029901](https://doi.org/10.1103/PhysRevC.85.029901))
142. Mueller TA et al.. 2011 Improved Predictions of Reactor Antineutrino Spectra. *Phys. Rev. C* **83**, 054615. ([10.1103/PhysRevC.83.054615](https://doi.org/10.1103/PhysRevC.83.054615))
143. Seo SH et al.. 2018 Spectral Measurement of the Electron Antineutrino Oscillation Amplitude and Frequency using 500 Live Days of RENO Data. *Phys. Rev. D* **98**, 012002. ([10.1103/PhysRevD.98.012002](https://doi.org/10.1103/PhysRevD.98.012002))
144. Adey D et al.. 2019 Extraction of the ^{235}U and ^{239}Pu Antineutrino Spectra at Daya Bay. *Phys. Rev. Lett.* **123**, 111801. ([10.1103/PhysRevLett.123.111801](https://doi.org/10.1103/PhysRevLett.123.111801))
145. de Kerret H et al.. 2020 Double Chooz θ_{13} measurement via total neutron capture detection. *Nature Phys.* **16**, 558–564. ([10.1038/s41567-020-0831-y](https://doi.org/10.1038/s41567-020-0831-y))
146. Kopeikin V, Skorokhvatov M, Titov O. 2021 Reevaluating reactor antineutrino spectra with new measurements of the ratio between ^{235}U and ^{239}Pu β spectra. *Phys. Rev. D* **104**, L071301. ([10.1103/PhysRevD.104.L071301](https://doi.org/10.1103/PhysRevD.104.L071301))
147. Sonzogni AA, Lorek RJ, Mattera A, McCutchan EA. 2023 Examination of decay heat measurements and their relevance for understanding the origin of the reactor antineutrino anomaly. *Phys. Rev. C* **108**, 024617. ([10.1103/PhysRevC.108.024617](https://doi.org/10.1103/PhysRevC.108.024617))
148. An FP et al.. 2017 Evolution of the Reactor Antineutrino Flux and Spectrum at Daya Bay. *Phys. Rev. Lett.* **118**, 251801. ([10.1103/PhysRevLett.118.251801](https://doi.org/10.1103/PhysRevLett.118.251801))
149. Bak G et al.. 2019 Fuel-composition dependent reactor antineutrino yield at RENO. *Phys. Rev. Lett.* **122**, 232501. ([10.1103/PhysRevLett.122.232501](https://doi.org/10.1103/PhysRevLett.122.232501))
150. Almazán H et al.. 2022 Joint Measurement of the ^{235}U Antineutrino Spectrum by Prospect and Stereo. *Phys. Rev. Lett.* **128**, 081802. ([10.1103/PhysRevLett.128.081802](https://doi.org/10.1103/PhysRevLett.128.081802))
151. Sonzogni AA, McCutchan EA, Johnson TD, Dimitriou P. 2016 Effects of Fission Yield Data in the Calculation of Antineutrino Spectra for $^{235}\text{U}(n,\text{fission})$ at Thermal and Fast Neutron Energies. *Phys. Rev. Lett.* **116**, 132502. ([10.1103/PhysRevLett.116.132502](https://doi.org/10.1103/PhysRevLett.116.132502))
152. Andriamirado M et al.. 2023 Final Measurement of the U235 Antineutrino Energy Spectrum with the PROSPECT-I Detector at HFIR. *Phys. Rev. Lett.* **131**, 021802. ([10.1103/PhysRevLett.131.021802](https://doi.org/10.1103/PhysRevLett.131.021802))
153. Bernstein A, Bowden N, Goldblum BL, Huber P, Jovanovic I, Mattingly J. 2020 *Colloquium: Neutrino detectors as tools for nuclear security.* *Rev. Mod. Phys.* **92**, 011003. ([10.1103/RevModPhys.92.011003](https://doi.org/10.1103/RevModPhys.92.011003))
154. Akindele O et al.. 2021 Nu Tools: Exploring Practical Roles for Neutrinos in Nuclear Energy and Security. ([10.2172/1826602](https://arxiv.org/abs/10.2172/1826602))
155. Acero MA et al.. 2022 White Paper on Light Sterile Neutrino Searches and Related Phenomenology. ([10.48550/arXiv.2203.07323](https://arxiv.org/abs/10.48550/arXiv.2203.07323))
156. Aker M et al.. 2022 Improved eV-scale sterile-neutrino constraints from the second KATRIN measurement campaign. *Phys. Rev. D* **105**, 072004. ([10.1103/PhysRevD.105.072004](https://doi.org/10.1103/PhysRevD.105.072004))
157. Aker M et al.. 2023 Search for keV-scale sterile neutrinos with the first KATRIN data. *Eur. Phys. J. C* **83**, 763. ([10.1140/epjc/s10052-023-11818-y](https://doi.org/10.1140/epjc/s10052-023-11818-y))
158. Esfahani AA et al.. 2022 The Project 8 Neutrino Mass Experiment. In *Snowmass 2021*. ([10.48550/arXiv.2203.07349](https://arxiv.org/abs/10.48550/arXiv.2203.07349))
159. Friedrich S et al.. 2021 Limits on the Existence of sub-MeV Sterile Neutrinos from the Decay of ^7Be in Superconducting Quantum Sensors. *Phys. Rev. Lett.* **126**, 021803. ([10.1103/PhysRevLett.126.021803](https://doi.org/10.1103/PhysRevLett.126.021803))

160. Martoff CJ et al.. 2021 HUNTER: precision massive-neutrino search based on a laser cooled atomic source. *Quantum Sci. Technol.* **6**, 024008. ([10.1088/2058-9565/abdb9b](https://doi.org/10.1088/2058-9565/abdb9b))
161. Bolton PD, Deppisch FF, Gráf L, Šimkovic F. 2021 Two-Neutrino Double Beta Decay with Sterile Neutrinos. *Phys. Rev. D* **103**, 055019. ([10.1103/PhysRevD.103.055019](https://doi.org/10.1103/PhysRevD.103.055019))
162. Hampel W et al.. 1998 Final results of the Cr-51 neutrino source experiments in GALLEX. *Phys. Lett. B* **420**, 114–126. ([10.1016/S0370-2693\(97\)01562-1](https://doi.org/10.1016/S0370-2693(97)01562-1))
163. Kaether F, Hampel W, Heusser G, Kiko J, Kirsten T. 2010 Reanalysis of the GALLEX solar neutrino flux and source experiments. *Phys. Lett. B* **685**, 47–54. ([10.1016/j.physletb.2010.01.030](https://doi.org/10.1016/j.physletb.2010.01.030))
164. Abdurashitov JN et al.. 1999 Measurement of the response of the Russian-American gallium experiment to neutrinos from a ^{51}Cr source. *Phys. Rev. C* **59**, 2246–2263. ([10.1103/PhysRevC.59.2246](https://doi.org/10.1103/PhysRevC.59.2246))
165. Abdurashitov JN et al.. 2006 Measurement of the response of a Ga solar neutrino experiment to neutrinos from an ^{37}Ar source. *Phys. Rev. C* **73**, 045805. ([10.1103/PhysRevC.73.045805](https://doi.org/10.1103/PhysRevC.73.045805))
166. Barinov VV et al.. 2022 Search for electron-neutrino transitions to sterile states in the BEST experiment. *Phys. Rev. C* **105**, 065502. ([10.1103/PhysRevC.105.065502](https://doi.org/10.1103/PhysRevC.105.065502))
167. Elliott SR, Gavrin VN, Haxton WC, Ibragimova TV, Rule EJ. 2023 Gallium neutrino absorption cross section and its uncertainty. *Phys. Rev. C* **108**, 035502. ([10.1103/PhysRevC.108.035502](https://doi.org/10.1103/PhysRevC.108.035502))
168. Goupy C et al.. 2023 Exploring coherent elastic neutrino-nucleus scattering of reactor neutrinos with the NUCLEUS experiment. *SciPost Phys. Proc.* **12**, 053. ([10.21468/SciPostPhysProc.12.053](https://doi.org/10.21468/SciPostPhysProc.12.053))
169. Augier C et al.. 2023 Results from a prototype TES detector for the Ricochet experiment. *Nucl. Instrum. Meth. A* **1057**, 168765. ([10.1016/j.nima.2023.168765](https://doi.org/10.1016/j.nima.2023.168765))
170. Singh V et al.. 2023 Large-area photon calorimeter with Ir-Pt bilayer transition-edge sensor for the CUPID experiment. *Phys. Rev. Applied* **20**, 064017. ([10.1103/PhysRevApplied.20.064017](https://doi.org/10.1103/PhysRevApplied.20.064017))
171. Saakyan R. 2023 Determination of absolute neutrino mass using quantum technologies. Symposium: Tritium Laboratory Karlsruhe – 30 years.
172. Vepsäläinen A et al.. 2020 Impact of ionizing radiation on superconducting qubit coherence. *Nature* **584**, 551–556. ([10.1038/s41586-020-2619-8](https://doi.org/10.1038/s41586-020-2619-8))
173. Cardani L et al.. 2021 Reducing the impact of radioactivity on quantum circuits in a deep-underground facility. *Nature Commun.* **12**, 2733. ([10.1038/s41467-021-23032-z](https://doi.org/10.1038/s41467-021-23032-z))
174. Wilen CD et al.. 2021 Correlated charge noise and relaxation errors in superconducting qubits. *Nature* **594**, 369–373. ([10.1038/s41586-021-03557-5](https://doi.org/10.1038/s41586-021-03557-5))
175. McEwen M et al.. 2022 Resolving catastrophic error bursts from cosmic rays in large arrays of superconducting qubits. *Nature Phys.* **18**, 107–111. ([10.1038/s41567-021-01432-8](https://doi.org/10.1038/s41567-021-01432-8))
176. Martinis JM. 2021 Saving superconducting quantum processors from decay and correlated errors generated by gamma and cosmic rays. *npj Quantum Information* **7**, 90. ([10.1038/s41534-021-00431-0](https://doi.org/10.1038/s41534-021-00431-0))